

# **Fabrication and Studies of Organic-Inorganic Hybrid Composites for Piezoelectric Based Vibration Sensors**

Swapnil Chetan Ghodke  
(MS11M03)

A Dissertation Submitted to  
Indian Institute of Technology Hyderabad  
In Partial Fulfillment of the Requirements for  
The Degree of Master of Technology



भारतीय प्रौद्योगिकी संस्थान हैदराबाद  
Indian Institute of Technology Hyderabad

Department of Materials Science and Engineering  
Indian Institute of Technology Hyderabad - 502205

July, 2013



## Declaration

I declare that this written submission represents my ideas in my own words, and where others' ideas or words have been included, I have adequately cited and referenced the original sources. I also declare that I have adhered to all principles of academic honesty and integrity and have not misrepresented or fabricated or falsified any idea/data/fact/source in my submission. I understand that any violation of the above will be a cause for disciplinary action by the Institute and can also evoke penal action from the sources that have thus not been properly cited, or from whom proper permission has not been taken when needed.



---

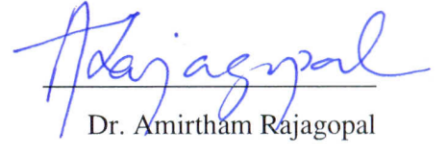
(Signature)

Swapnil Chetan Ghodke

MS11M03

## Approval Sheet

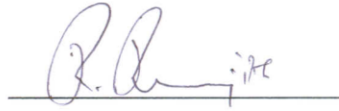
This thesis entitled “Fabrication and Studies of Organic-Inorganic Hybrid Composites for Piezoelectric Based Vibration Sensors” by Swapnil Chetan Ghodke is approved for the degree of Master of Technology from IIT Hyderabad.



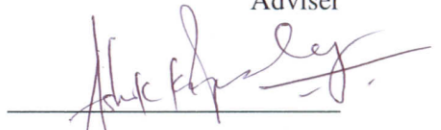
Dr. Amirtham Rajagopal  
Assistant Professor  
Department of Civil Engineering  
Examiner



Dr. Bharat Bhooshan Panigrahi  
Assistant Professor  
Department of Materials Science and Engineering  
Examiner



Dr. Ranjith Ramadurai  
Assistant Professor  
Department of Materials Science and Engineering  
Adviser



Dr. Ashok Kumar Pandey  
Assistant Professor  
Department of Mechanical Engineering  
Chairman

## Acknowledgements

It was my dream to study in one of the premier institute and that came true after joining Department of Materials Science and Engineering at IIT Hyderabad. It was a wonderful journey which have given me an opportunity to explore myself.

One of the best thing happened in my life is to work on my M.tech thesis under the guidance of **Dr. Ranjith Ramadurai**, Assistant professor, Department of Materials Science and Engineering, IIT Hyd. His excellent guidance, motivation and inspiration have continuously helped me to complete my research work. I am thankful of him for giving me a life time opportunity to work with him and FMRG group.

I want to thank **Dr. Pinaki Bhattacharjee** H.O.D, Department of materials science & engineering, IIT Hyd and all my faculty for giving world class education.

I also want thank **Dr. Amritham Rajagopal**, Assistant professor, Department of Civil Engineering, IITH for giving me access to civil dept. labs to carry out my experiments.

I would like to show my sincere thanks to all Phd scholars of Dept. of Materials Science and Engineering, IIT Hyd., Physics Department, IIT Hyd specially **Mr. Mallesh, Mr. Akki, Mr. Karthik, Mr.Damodar, Mr. Venkat, Mr. Deepak** for helping me to complete my experiments and sharing their knowledge and also I am thankful for giving me access to chemistry Lab, Electrical Lab, Nano-X Lab. to carry out my experiments for research work.

I want to thank all my friends for being my constant source of motivation and special thanks to **Mr. Rajdatta, Mr. Ashish, Mr. Alok, Mr Anubhav, Mr Bhupendra** for being with me in my good as well as bad time and thanks for making my days in IIT H memorable.

Lastly I acknowledge the benelovance of my family for their constant love, encouragement, blessings and support during my study.

Dedicated to

My guide Dr. Ranjith Ramadurai,  
My family and My friends

## Abstract

Piezoelectric polymers and ceramics are widely studied for their promising applications in actuators and sensor technologies. Polyvinylidene Fluoride (PVDF) is a piezoelectric polymer which is extensively studied due its piezoelectric response, chemical and mechanical durability. However, the inherent drawback associated with functional polymers is a poor electromechanical coupling. Though piezoelectric ceramics possess high electromechanical coupling they are brittle and not suitable for certain applications. Hence, organic-inorganic functional composites are believed to overcome both drawback of weak coupling in polymer and high brittleness of ceramics. There have been extensive studies on PVDF-lead based piezo composites, however, a lead free inorganic piezoelectric is preferred due to the environmental friendly requirements.

The thesis deals with synthesise and studies of hybrid composite consisting sodium bismuth titanate  $\text{Na}_{0.5}\text{Bi}_{0.5}\text{TiO}_3$  (NBT) as dispersed phase and PVDF film as matrix. NBT is a lead free piezoelectric ceramic material with high ferroelectric to paraelectric transition temperature ( $\sim 320^\circ\text{C}$ ) and PVDF polymer films are semi crystalline with Curie temperature  $103^\circ\text{C}$ . PVDF is conventionally known to possess  $\alpha$ ,  $\beta$ ,  $\gamma$ ,  $\delta$  phases. The  $\beta$ -phase of PVDF is desirable as it possess high polarizability. Initially, NBT ceramic powders and PVDF thick films were individually synthesized and characterized for obtaining optimized piezoelectric and ferroelectric properties. Later, composite films of different weight percentage of NBT and PVDF matrix were synthesized. The composite was aimed at utilization of smart structures mainly for vibration sensor applications. Though composite is the final aimed product NBT of its own is not a well-studied compound and hence a detailed vibration response of NBT ceramics was also studied. Hence the individual constituents were studied in details for their physical and functional properties aiming at a PVDF-NBT composite thick films for piezoelectric applications.

## **Nomenclature**

NBT - Sodium bismuth titanate

PVDF - Polyvinylidene Fluoride

$\epsilon$  - Dielectric constant

$\gamma$ - Diffusivity

$\lambda$ - Wave length

$T_c$  - Curie temperature

$d$  - Inter planer spacing in crystal

$a, b, c$  - Crystal unit cell parameter

RT- Room temperature

SEM Scanning electron microscope

XRD X-ray diffraction



# Contents

Declaration .....	<b>Error! Bookmark not defined.</b>
Approval Sheet .....	<b>Error! Bookmark not defined.</b>
Acknowledgements .....	iv
Abstract .....	vi
<b>Nomenclature .....</b>	<b>vii</b>
<b>1 Introduction .....</b>	<b>1</b>
1.1 Overview.....	1
1.2 Piezoelectricity.....	2
1.3 Piezoelectric materials.....	4
1.4 Basic piezoelectric constants.....	5
1.5 Motivation and Objectives.....	7
<b>2 Literature Survey.....</b>	<b>8</b>
2.1 Piezoelectric ceramics.....	8
2.1.1 Sodium Bismuth Titanate .....	8
2.1.2 Phase transformation in NBT .....	9
2.1.3 Piezoelectric properties of NBT.....	10
2.1.4 Limitations for NBT.....	10
2.1.5 Synthesis route.....	11
2.2 Piezoelectric polymers .....	12
2.2.1 Poly (Vinylidene fluoride).....	12
2.2.2 Properties of PVDF .....	13
2.3 Piezoelectric composite .....	14
<b>3 Experimental Details.....</b>	<b>16</b>
3.1 Synthesis of NBT ceramic.....	16
3.1.1 Solid state reaction route.....	16
3.1.2 Steps of solid state reaction.....	17

3.2 Synthesis of PVDF thick films.....	23
3.3 Synthesis of PVDF/NBT composite films.....	26
3.4 Characterization techniques.....	27
3.4.1 X-ray diffraction.....	27
3.4.2 Scanning electron microscopy.....	28
3.4.3 Dielectric studies.....	28
3.4.4 Raman Spectroscopy.....	30
3.4.5 Mechanical behavior of Composite and PVDF thick films.....	30
<b>4 Results and Discussion.....</b>	<b>31</b>
4.1 Results and discussion on NBT ceramic.....	31
4.1.1 Structural analysis of NBT.....	31
4.1.2 Morphological studies of NBT by SEM.....	34
4.1.3 Physical property studies on NBT.....	34
4.2 Results and discussion of PVDF polymer and PVDF/NBT composite.....	41
4.2.1 Structural analysis of PVDF and PVDF/NBT composite.....	41
4.2.2 Morphological studies of PVDF and PVDF/NBT composite films by SEM.....	45
4.2.3 Mechanical behavior of PVDF/NBT composite material.....	46
<b>5 Studies on NBT as a Vibration Sensor.....</b>	<b>48</b>
5.1 Introduction.....	48
5.2 Experimental setup.....	49
5.3 Results of vibration sensor.....	50
5.4 Conclusion.....	51
<b>6 Summary and Conclusion.....</b>	<b>52</b>
6.1 Summary.....	52
6.2 Conclusions.....	52
6.3 Future work.....	53

## References

# Chapter 1

## Introduction

### 1.1 Overview

Over a century the research and development on dielectric materials have grown up exponentially. Every work in this field has revolutionized the technology for the welfare of human being. These materials have shown application in wide range such as in capacitors, optical shutters and modulators, computer memory and display, microwave communication devices, piezoelectric detectors, ferroelectric random access memory etc. Dielectric materials can be defined as insulating materials, which are very poor conductor of electric current. Especially dielectrics are known for generating electric polarization when they are kept in electric field because of absence of loosely bonded or free electrons. Where polarization is charge per unit area of material or dipole moment generated per unit volume. The broad classification or the inter relationship of different kind of materials is shown in Fig. 1.1

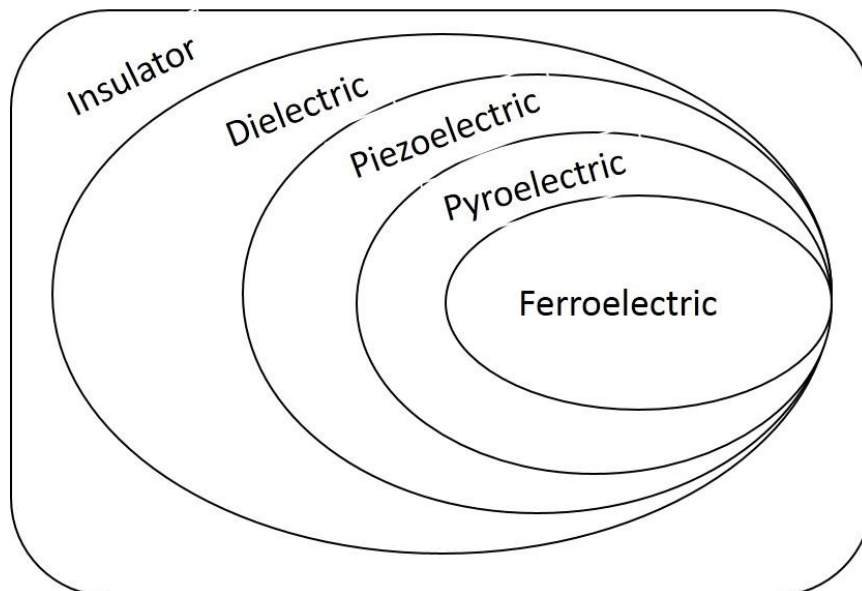


**Fig.1.1: Classification of insulating materials**

#### 1. Ferroelectric Materials

Ferroelectric domains are the regions where electric dipoles in it are aligned in particular direction. They possess a polarization hysteresis loop under electric field and most importantly they possess a polarization reversal property.

2. Pyroelectric materials

The material that polarizes when subjected to change in temperature.

3. Piezoelectric materials

The materials shows coupling between mechanical and electrical energy. Mechanical stress produces surface charge/polarization and under electric field it generates mechanical strain.

### 1.2 Piezoelectricity

Piezoelectricity is linear interaction between mechanical and electrical systems in non-centric crystals or similar structures. Generation of charge on application of mechanical stress is direct piezoelectric effect and was discovered in quartz by Pierre and Jacques Curie in 1880. In response to electric field material shows mechanical deformation called as converse piezoelectric effect, discovered by Gabriel Lippmann in 1881 [1].

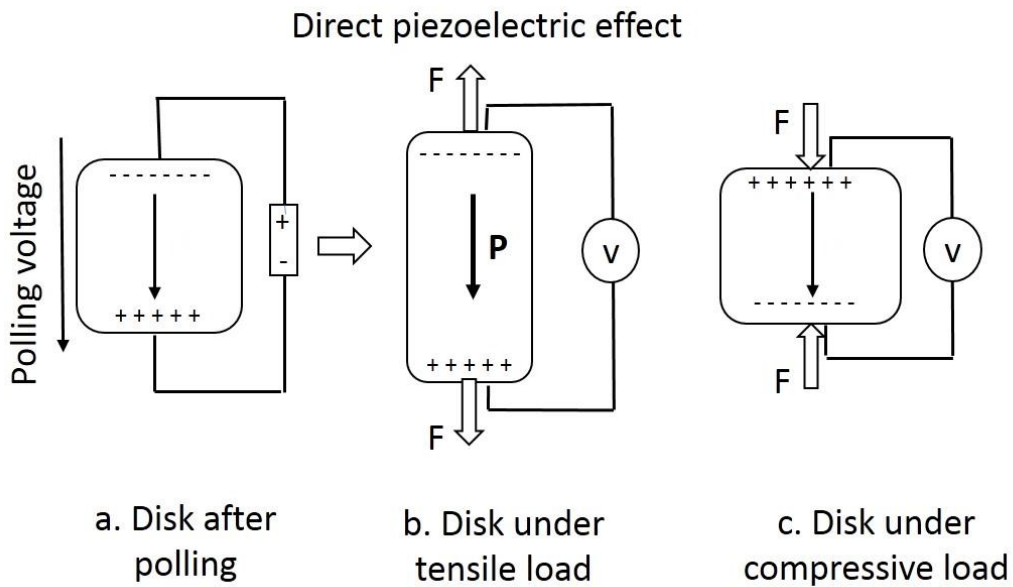
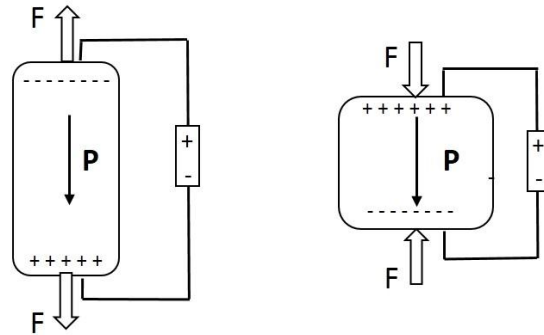


**Fig 1.2: Schematic representation of direct piezoelectric effect.**

Converse piezoelectric effect



d. Elongation due to applied voltage

e. Contraction due to applied voltage with opposite polarity

**Fig. 1.3: Schematic representation of converse piezoelectric effect.**

The piezoelectric property of a material is purely related to the atomic arrangement; the information related to atomic arrangement can be clearly understood from the crystallography.

Crystallography consist 7 crystal systems based on periodicity of atomic arrangement, which are classified into 14 Bravais lattices. Further, these 7 crystal systems are classified into 32 crystal classes known as point groups.

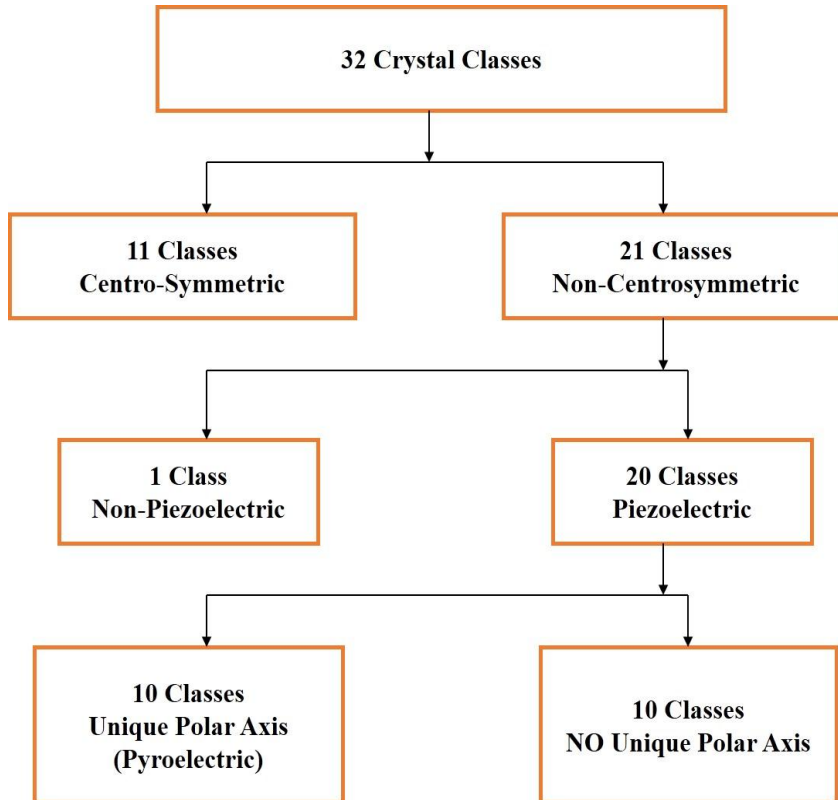


**Fig. 1.4: Schematic representation of the classification of point groups**

Among them, 11 point groups non-polar due to centrosymmetric. The other 21 point groups out of the 32 point groups are non-centrosymmetric. All non-centrosymmetric except 432 exhibit piezoelectric effect. They get polarized by applying mechanical stress. The systematic representation is given in the Fig. 1.5 given below. The non-centrosymmetric structures are known as perovskites. The general chemical formula for perovskite compounds is  $ABO_3$ , where 'A' and 'B' are two cations of different size, and 'O' is an anion, which makes bonds with both A and B. The valence of the A cation ranges from +1 to +3 and the B cation from +3 to +6. The 'A' atoms are larger than the 'B' atoms. The perovskite structure consists of corner shared oxygen octahedral with B site cation in the middle. The A cations are situated at interstitial sites created by oxygen octahedral.

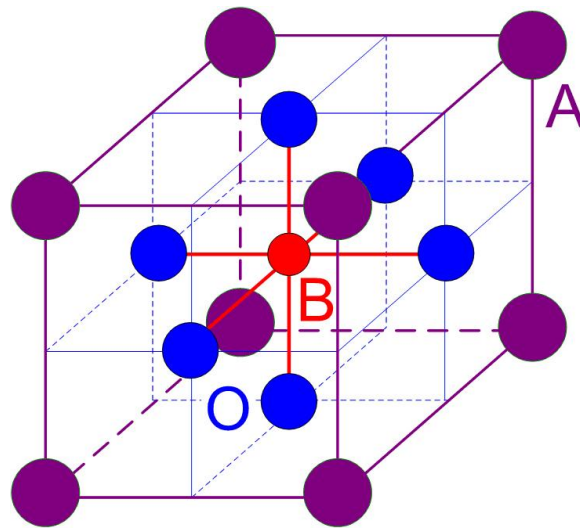


Fig. 1.5 The schematic representation of perovskite lattice structure [2]

### 1.3 Piezoelectric materials

- Single crystal materials: Quartz, Lithium niobate ( $LiNbO_3$ ), and Lithium tantalite ( $LiTaO_3$ )
- Piezo-ceramics: Barium titanate ( $BaTiO_3$ ), Lead titanate ( $PbTiO_3$ ), Lead zirconate titanate ( $PbZrTiO_3$ ) - More commonly known as *PZT*, *NBT*.
- Piezo-polymers: Polypropylene, Polystyrene, Poly(vinylidene fluoride) (*PVDF* or *PVF<sub>2</sub>*)
- Piezo-composites: Combination of Piezoelectric ceramics and polymers Example *PVDF-PZT*, *PVDF-BT*, etc [3]

## 1.4 Basic piezoelectric constants

### I. Piezoelectric charge constant (**d**) :

“The polarization generated per unit of mechanical stress applied on material”

$$d_{ij} = \frac{\text{short circuit charge density}}{\text{Applied mechanical stress}}$$

$d_{ij}$ : “i” subscript means direction of polarization and j second subscript means direction of applied mechanical stress. Example  $d_{33}$  means induced polarization in direction 3 (Parallel to direction in which ceramic element is polarized) per unit stress applied in direction 3

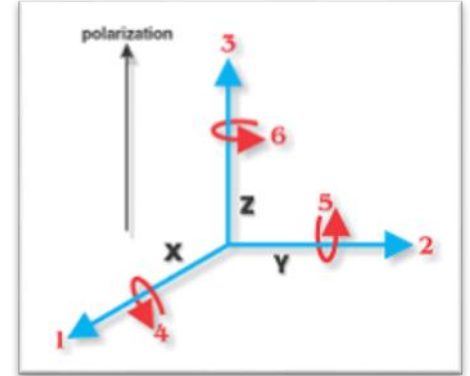


Fig. 1.6: Reference coordinate for representing piezo constants [4]

### II. Piezoelectric voltage constant (**g**)

“The electric field generated by a piezoelectric material per unit of mechanical stress applied “

$$g_{ij} = \frac{\text{Electric field generated}}{\text{Applied mechanical stress}}$$

$g_{33}$  : Means induced electric field in direction 3 (parallel to direction in which ceramic element is polarized) per unit stress applied in direction 3

### III. Electromechanical coupling factor (**k**)

“Indicator of the effectiveness with which a piezoelectric material converts electrical energy into mechanical energy, or converts mechanical energy into electrical energy”

Coupling factor can be calculated from the resonance frequency. The resonance frequency for a material is the frequency at which material converts electrical energy to mechanical or vice versa most efficiently. Fig.1.7 show the frequency vs. impedance plot. Where  $f_m$  is frequency at minimum impedance and  $f_n$  as frequency of maximum impedance. Maximum response from the element will be at a point between  $f_m$  and  $f_n$  and for the graph of capacitance vs. frequency it will become completely reverse as capacitance is inversely proportional to impedance but the values of minimum and maximum frequencies will be the same.

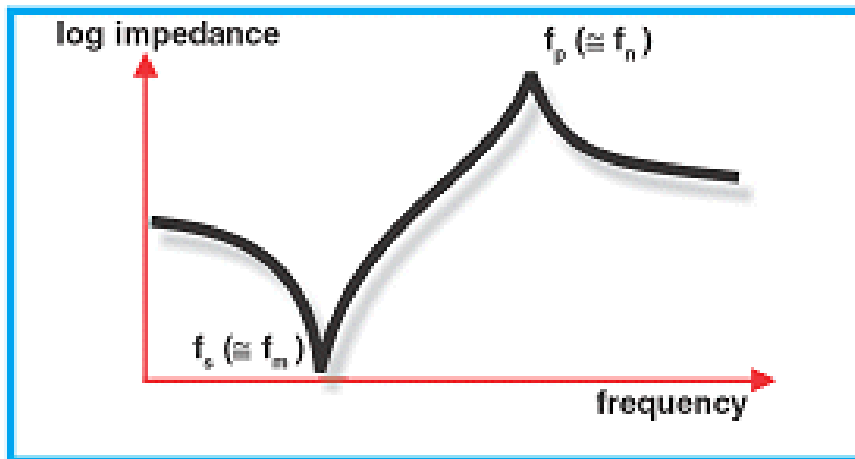


**Fig. 1.7 showing maximum and minimum resonance frequencies [4]**

Coupling Factor for Discs shape sample (surface is much larger than the thickness) is given by formula mentioned below.

$$k_p = \sqrt{\left[\left(\frac{2.51(f_n - f_m)}{f_n}\right) - \left(\frac{f_n - f_m}{f_n}\right)^2\right]} \dots\dots\dots 1.1$$



## 1.5 Motivation and Objectives

### Motivation:

- Lead based piezoelectric materials are commercially used for sensors and actuators: The European Community in 2006 started RoHS (Restrictions on the use of certain Hazardous Substances), which explicitly limits the usage of lead (Pb) in electronic equipment as lead is Toxic it hazardous for environment and human life.[1]
- Lead free piezoelectric materials have shown comparable piezoelectric properties such as  $BaTiO_3$ ,  $KNbO_3$ ,  $Na_{0.5}Bi_{0.5}TiO_3$  (NBT), Bismuth layered compounds , tungsten based compounds and PVDF based composites.[3]
- In spite of the interesting properties exhibited by piezoelectric materials the major factor that decides the utilization of a piezoelectric for the applications is the electromechanical strain coupling present in the material. In the case of ceramics the electromechanical coupling coefficients are relatively higher and ranges between 45-65% of coupling [5]. In the case of polymer piezoelectric materials it ranges between 10-35% [6]. However, the brittleness of ceramics comes as hindrance to utilize them in various applications and in addition they cannot be fixed along the surface of complex shapes, due to the absence of flexibility.
- Hence, in recent years there have been several approaches to introduce in-organic and organic based hybrid piezoelectric materials to utilize them for smart structure applications. Hence synthesis and studies of hybrid composites for piezoelectric applications has gained interest aiming at smart structure applications.

### Major Objectives:

- Synthesis of NBT ceramics through solid state reaction techniques which is a lead free piezoelectric material and considered as a potential alternate for lead based piezoelectric materials.
- Synthesis of PVDF by solution casting method and study its mechanical and piezoelectric properties
- Synthesis of PVDF-NBT composite by solution casting and study its mechanical and piezoelectric properties.
- Demonstrate piezoelectric response of fabricated device.

# Chapter 2

## Literature survey

### 2.1 Piezoelectric ceramics

The first reported piezoelectric ceramic is Rochelle salt by Jacques and Pierre Curie after that plenty of piezoelectric ceramics were discovered and studied for its applications. The piezoelectric ceramic have unique structure to poses piezoelectricity phenomenon. This structure are mainly categorized as non-centrosymmetric which are made up of mixed oxides with corner-sharing octahedra of  $O^{2-}$  ions. This materials can be called as perovskites ( $ABO_3$ ) where A = Na, K, Rb, Ca, Sr, Ba, Pb, etc. and B = Ti, Sn, Zr, Nb, Ta, or W. The common examples are barium titanate ( $BaTiO_3$ ), lead titanate ( $PbTiO_3$ ), lead zirconate titanate (PZT), lead lanthanum zirconate titanate (PLZT), and lead magnesium niobate (PMN) [7]. Piezoelectric ceramics have high electromechanical coupling, high dielectric constant and high  $d_{33}$  coefficient. Despite the excellent ferroelectric and piezoelectric properties of lead based ferroelectric materials, these materials contain a large amount of lead (> 60 wt. %) which is toxic [8].

#### 2.1.1 Sodium Bismuth Titanate (NBT)

The lead based materials are being regulated for electronic applications as they are hazardous and toxic in nature. So the researcher from all over the globe are focusing on lead free materials. One of the prominent material is Sodium bismuth titanate ( $Na_{0.5}Bi_{0.5}TiO_3$ ), which was discovered by Smolenski et al in 1961 [9]. Sodium bismuth titanate is an A-Site substitute distorted perovskite ( $ABO_3$ ) compound [9]. Compounds analogous to NBT are  $Ag_{0.5}Bi_{0.5}TiO_3$  (Park et al., 1999),  $K_{0.5}Bi_{0.5}TiO_3$  (Smolenskii et al., 1960),  $Ag_{0.5}Nd_{0.5}TiO_3$  (Park et al., 1998) and the rare-earth manganites typified by  $La_{0.5}Sr_{0.5}MnO_3$  (Woodward et al., 1998) [10].

Reasons for NBT being one of the superior lead free compounds for piezoelectric applications are

- i. Exhibits strong ferroelectric properties at room temperature
- ii. High remnant polarization  $38\mu C/cm^2$
- iii. High curie temperature  $320^{\circ}C$

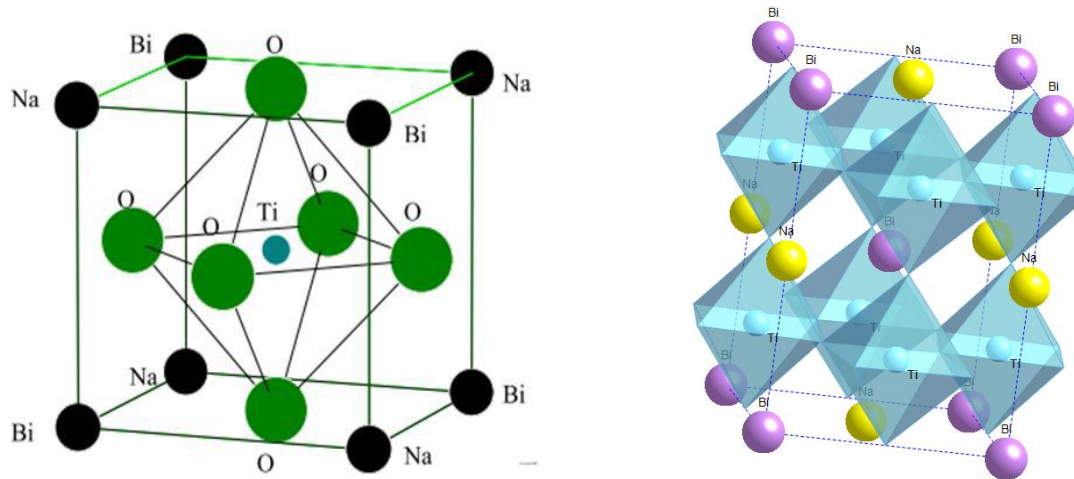
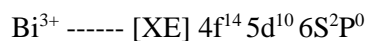
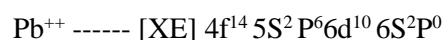


**Fig. 2.1 NBT (Perovskite) crystal structure [11]. B (Right) Schematic of the pseudo-cubic NBT perovskite structure [12].**

The major motivation to do research on NBT compounds lies in its electronic configuration. In lead based systems for piezoelectricity  $Pb^{2+}$  is responsible for high polarization due to its lone pair effect of 6S valance shell electron. Similarly in NBT  $Bi^{3+}$  has a similar configuration as lead.



### 2.1.2 Phase transformations in NBT

NBT is ferroelectric with a rhombohedral (R3C) structure at room temperature and exhibits temperature dependent phase transformations. On heating first transformation is ferroelectric to antiferroelectric which occurs near to 200°C, this temperature is also called as depolarization temperature as piezoelectricity vanishes above this temperature [13].

Second transformation is antiferroelectric to paraelectric transformation occurs at ~320°C which is diffusive in nature [14]. Saradhi *et al* [14] reported that NBT is strongly ferroelectric below 200 °C and in between 200 and 320 °C it is antiferroelectric in nature.

NBT also exhibits relaxor features with long range ferroelectric ordering than other classical relaxors [14]. Tu et al also spoke about relaxor behavior of NBT due to super paraelectric micro polar structure. The overall picture relating to structural phase transition behavior and physical properties are inconsistent and needs more study to resolve it [15]. The relaxor nature of NBT can be described by modified Curie-Weiss law.

$$\left(\frac{1}{\varepsilon} - \frac{1}{\varepsilon_m}\right) = (T - T_m)^\gamma / C'$$

Where  $\gamma$  is the diffusivity,  $C'$  is the Curie Weiss constant,  $\varepsilon$  is dielectric constant at a temperature  $T$  and  $\varepsilon_m$  is dielectric constant at  $T_c$ . The value of  $\gamma$  (diffusivity) is calculated from the slope of  $\log(1/\varepsilon - 1/\varepsilon_m)$  versus  $\log(T - T_m)$  plot. The diffusivity ( $\gamma$ ) varies between 1 and 2,  $\gamma = 1$  means material obeys normal Curie-Weiss law with normal paraelectric to ferroelectric transition. The Complete diffuse phase transition means  $\gamma = 2$  [14].

### 2.1.3 Piezoelectric properties of NBT

The reported results for hysteresis behavior of NBT show high coercive field of 73kV/cm and large remnant polarization 38 $\mu$ C/cm<sup>2</sup> [15-17] and  $d_{33}$  of 125pC/N.

### 2.1.4 Limitations for NBT

The main drawback is its high coercive field i.e. 73kV/cm which requires high electric fields in poling and which comparatively lower than the commercial piezoelectric material. The important technique to overcome this problem is to dope a substitute at a site or make a composite so that it will lower its coercive field and improve its  $d_{33}$  coefficient. So to improve the properties the solid solutions such as NBT-BKT [18], NBT-BT [19,20], NBT- SrTiO<sub>3</sub> [21], NBT- BiFeO<sub>3</sub> is been reported. The NBT is typically shown as ordered structure of Bi and Na cations at A site in ABO<sub>3</sub> perovskite form but it is not true. The A site ordering in the structure is expected to be on smaller physical length scales.

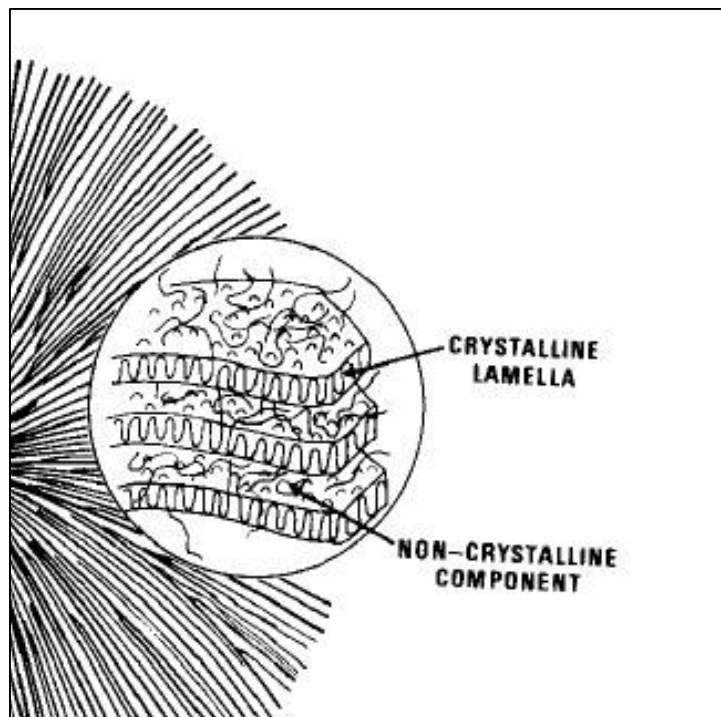
### 2.1.5 Synthesis routes

NBT can be synthesized through solid state reaction route, hydrothermal technique, molten salt bath technique, sol gel method. The solid state reaction route gives phase pure polycrystalline NBT material with density of about 90%. Thus solid state route for synthesis is easy, cheap and effective for NBT synthesis. Hence, in this work we have adopted for solid state synthesis route.

## 2.2 Piezoelectric polymers

There are very few polymer which exhibits piezoelectric property. The commonly known piezoelectric polymers are Polyvinylidene fluoride (PVDF) which is most commonly used, Copolymers of polyvinylidene fluoride with trifluoroethylene (TrFE) and tetrafluoroethylene (TFE), Polyamides, Liquid-crystalline polymers, Biopolymers etc. This piezoelectric polymer show wide range of applications mainly in making in devices which are used in medical instrumentation, robotics, optics, computers, and ultrasonic, underwater and electroacoustic transducers [23]. The mechanism of piezoelectricity in polymers is in the semi-crystallinity. The morphology of semicrystalline polymer consist polar crystallites dispersed in amorphous region as shown in Fig. 2.2

**Fig 2.2 Schematic diagram of PVDF semi-crystalline structure [23].**



### 2.2.1 Poly (Vinylidene fluoride)

PVDF was discovered by Dr. Heiji Kawai, in 1969 [24]. Piezoelectric nature to PVDF was proved by Furakawa and Johnson in 1981. The Curie point of PVDF is 103°C. PVDF possess  $\alpha$ ,  $\beta$ ,  $\gamma$  and  $\delta$  as four different phases, among them  $\beta$  phase have the most responsive piezoelectric properties. Compare to all ferroelectric polymers PVDF have dielectric constant with good chemical and mechanical durability. In general the physical properties of PVDF make it most valuable material for application in sensors.

The table 2.1 one compares the properties of piezoelectric ceramic and polymers. Here in table polymers shows dominating properties for piezoelectric application but the main drawback it possess is low dielectric constant and low piezoelectric constant so it can be applicable for sensor part but not the actuator.

Property	Piezoelectric Polymers	Piezo Ceramics
Actuation Strain	2-5%	0.1-0.3%
Actuation Force (MPa)	0.1-3	30-40
Density	1-2.5 g/cc	6-8 g/cc
Power Consumption	m-Watts	Watts
Relative Toughness	Resilient, Elastic	Brittle

**Table 2.1: Comparison between piezoelectric ceramic and polymer**

### 2.2.2 Properties of PVDF

PVDF is typically a semi crystalline polymer with approximately 50% crystallinity due to repeating unit of  $-(CH_2-CF_2)-$ . PVDF is conventionally known to possess  $\alpha$ ,  $\beta$ ,  $\gamma$  and  $\delta$  as different phases, where  $\alpha$ -PVDF occurs in a trans-gauche-trans-gauche (TGTG) formation. Where T represents a trans bond that remains in the same plane as the carbon backbone. The G's represent the bonds that skew the carbon backbone from the plane. Each G or G- bond represents a  $60^\circ$  or  $-60^\circ$  angle respectively from the plane of the last bond.

The  $\beta$  crystal phase of PVDF forms a planar zigzag, or TT where T represents a trans bond that remains in the same plane as the carbon backbone. This crystal structure also allows more dipolar alignment giving the polymer its strong piezoelectric properties.

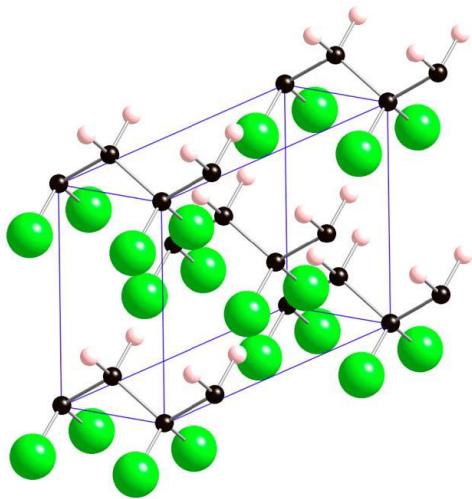


Fig 2.3 Schematic representation of  $\beta$ -PVDF [25]

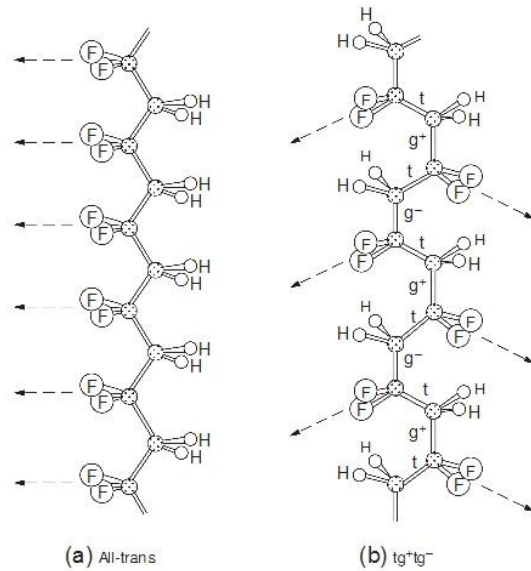


Fig 2.4: Structure of  $\alpha$  PVDF (right) and  $\beta$  PVDF (left)[26]

The  $\beta$  phase is also an orthorhombic unit cell with lattice constants of  $a=8.45$ ,  $b=4.88$ , and  $c=2.55$  Å and has a density of  $1.8$  g/cm<sup>3</sup>. The all-trans conformation of the carbon backbone, and parallel arrangement of the chains in the crystalline unit cell creates a net charge in the  $\beta$  phase structure of PVDF. Randomly arranged dipoles in  $\beta$ -PVDF gives zero net polarization. However, after poling process it show strong polarization [27].

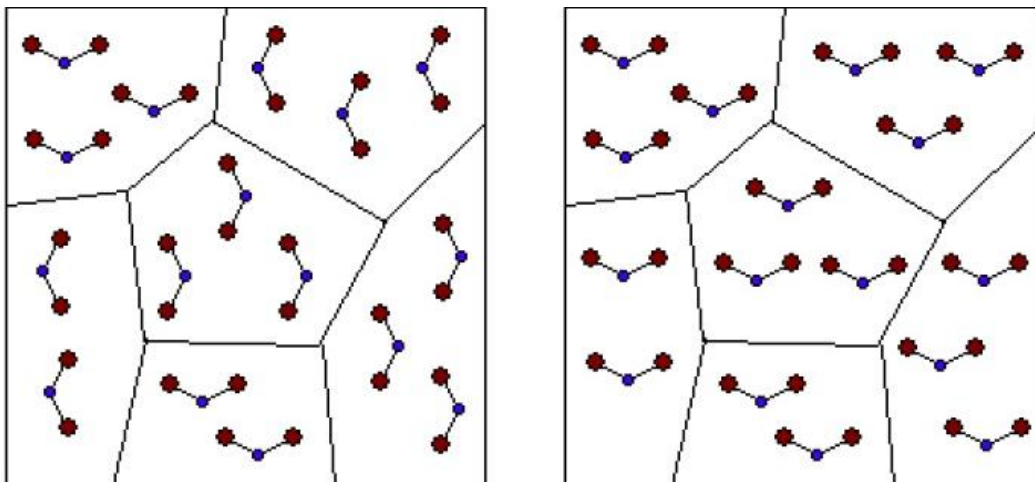


Fig 2.5 shows randomly oriented dipoles in left and aligned dipoles after poling process [27]

The following are different ways to obtain  $\beta$  phase

- I. Through mechanical drawing of the  $\alpha$  phase
- II. Solution cast from a solution of polar solvents. Depending on the temperature of evaporation, the resulting film will be either  $\alpha$  or  $\beta$ .
- III. Depositing on special substrate
- IV. By incorporating Halide, carbon tubes, carbon fibers or nanoclay [28]

Disadvantages

- i. Drawing of PVDF film creates irregularities and defects in the film.
- ii. Impossible to draw film formed on substrate

### 2.3 Piezoelectric composite

Every material has its own advantages and drawbacks for practical application. Such as polymers have good flexibility, low acoustic impedance but low dielectric constant. Whereas ceramic have good electromechanical coupling coefficient less expensive and easy in synthesis but they are brittle suffers from poor mechanical strength, have high acoustic impedance so are limited for design of flexible material.

The composite with above extraordinary properties can be used for capacitors, electric energy storage devices. Researchers have studied combination by three different routes. First is both matrix and ceramic as ferroelectric material example: PVDF with ferroelectric ceramic  $\text{Pb}(\text{Zr,Ti})\text{O}_3$  (PZT)[29],  $\text{Pb}(\text{Mg}_{1/3}\text{Nb}_{2/3})\text{O}_3 - \text{PbTiO}_3$  (PMNPT),  $\text{BaTiO}_3$  (BT) and a three phase composite of (BT+PVDF) with carbon fiber is also reported by Zang et al [30]. Second is ferroelectric ceramic with non-ferroelectric polymer and third is ferroelectric polymer with non-ferroelectric ceramic such as  $\text{CaCu}_3\text{Ti}_4\text{O}_{12}$  (CCTO) [31], PVDF/nano- $\text{TiO}_2$  [32], PVDF/graphite, PVDF/ZnO [33]. The composite were manufactured in various manner such particulate composite, fiber reinforced composite, multilayered composite by solution casting or by melt casting, Injection moulding [34]. The piezoelectric properties depends on the elastic and electric energies distributed between the materials.



Material	Piezo Constant (pC/N)	Piezo Strain/Volt (Vm/N x 10 <sup>-3</sup> )
BaTiO <sub>3</sub>	191	12.6
Quartz	2.3	50.0
PZT	289	25.1
PVDF	-33	-339
NBT	125	---

**Table 2.2 Comparison between piezoelectric materials [27]**

Table 2.2 shows the comparison of piezoelectric properties of commonly used piezoelectric materials. Among them PZT is lead based, Quartz is having very low piezo constant, BaTiO<sub>3</sub> shows transition at room temperature and except PVDF/NBT composite all combinations are extensively studied. So combination of PVDF and NBT can give good piezoelectric properties.

# Chapter 3

## Experimental Details

The work of the project is focused on synthesis and characterization of composite material for piezoelectric application. The constituents for the composite are sodium bismuth titanate (NBT) and PVDF. Hence, initially the prime objective was to synthesize and characterize them individually and obtain optimal properties.

### 3.1 Synthesize of NBT ceramic

Sodium bismuth titanate ( $\text{Na}_{0.5}\text{Bi}_{0.5}\text{TiO}_3$ , NBT) is a ferroelectric ceramic material which can be synthesized as single crystal, sintered pellets or as powder form. Considering that the composite is a particulate composite it was decided to prepare NBT ceramic in powder form. It is essential to control the composition, structure and variable parameters. Following are some general methods used for synthesis of ceramic

1. Mechanical methods
  - a. Solid state reaction
  - b. High energy ball milling
2. Chemical methods
  - a. Sol- gel method
  - b. Co-precipitation method
  - c. Hydrothermal synthesis
  - d. Combustion method

In spite of the disadvantage of inhomogeneity and low density the mechanical methods are preferred because of their easy and fast output for large scale production of bulk ceramic powder. In this project we adopted the solid state reaction route to synthesize NBT powders.

#### 3.1.1 Solid state reaction route

The solid state reaction route is the most convenient method for the preparation of polycrystalline solids from a mixture of solid oxide and carbonates as precursors. The reaction occurs at high temperature so the thermodynamic energy determines the feasibility of the reaction. The rate of reaction depends upon reaction conditions, structural properties of the reactants, surface area of the solids and their reactivity.

The heat in the reaction decomposes the precursors into fragment for direct combination. The high temperature act as driving force for diffusion of the atoms. The rate of reaction can be increased by reaching to the temperature were one of the precursor starts to melt as this will help in overcoming the solid state diffusion barrier. Proper mixing and grinding of precursors is mandatory to increase the surface energy of the reactants and reduce the reaction time and facilitate phase formation.

### 3.1.2 Steps of solid state reaction

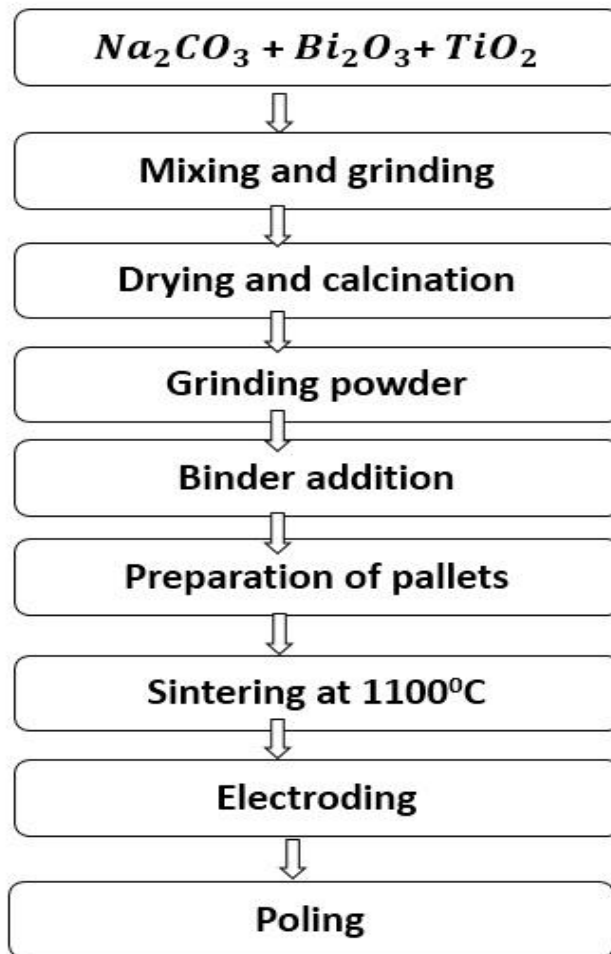


Fig 3.1: Flow chat for NBT synthesis through solid state reaction

#### I. Selection of Precursors

The raw materials for the reaction are selected on the basis of desired product. The quality of raw materials depends upon the purity percentage and particle size. The physical properties such as melting point, surface area, purity of precursors decides the operating conditions for the reaction to get the purest form of final product.

Precursors are sodium carbonate( $\text{Na}_2\text{CO}_3$ ) bismuth oxide ( $\text{Bi}_2\text{O}_3$ ) and titanium oxide ( $\text{TiO}_2$ ) all are 99.99% pure manufactured by Sigma Aldrich.

## II. Weighing and Mixing

To maintain the stoichiometric ratio is very important so the precursors are measured carefully based on the reaction given below.



For synthesis of 1gram of NBT powder following amount of reagents are needed

- a) Sodium carbonate – 0.125gm
- b) Bismuth oxide – 0.5498gm
- c) Titanium oxide – 0.37699gm

Precursors are manually grinded for one hour in agate mortar and pestle with acetone as volatile liquid medium. The wet grinding process mix the reagents homogeneously and make the particle surface thermodynamically active for reaction. Then the mixture was kept for drying at room temperature.

## III. Calcination

The calcination process is an endothermic decomposition reaction which gives oxide as a solid product and liberates gases. Calcination is used to achieve the desired crystal phase and particle size [35]. The dried and mixed powder was calcined at three different temperatures to study the time and temperature dependent effect on phase formation of NBT. The mixture was calcined at  $750^\circ\text{C}$ ,  $800^\circ\text{C}$  and  $850^\circ$  and the time was varied from two to four hours. One of the calcination cycles is show in fig.3.1. After calcination process the powder was again grinded for one hour and was checked for phase formation by powder X-ray diffraction at room temperatures.

The powder was then ball milled for 12hs with 400 rpm speed, 24 cycles (one cycle = 15 min. grinding + 15min. halt).

The balling is also wet grinding where propanol is used as liquid. In this process 7ml of propanol was used for 4 grams of NBT powder with 9 agates balls.

The fine powder obtain was heated in oven for an hour at  $100^\circ\text{C}$  to remove the moisture/Acetone contain.

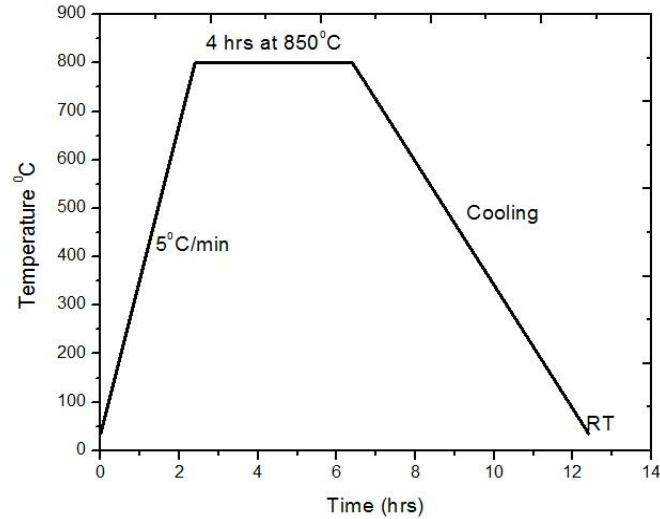


**Fig. 3.2: Calcination cycle of the homogeneous mixture for NBT phase formation**

#### **IV. Pellet making**

The calcined powder was then mixed properly by grinding powder with few drops of 2%PVA (Polyvinyl Alcohol) binder. The circular shape die of diameter 8mm was used to make the pellets. Before compacting the powder, the die was cleaned with citric acid to avoid the plunger to get stuck in the die. The pressure of 390 MPa was applied by Cold hydrostatic press for making a sample of 2mm thickness. The image of hydraulic press is show in Fig. 3.3



**Fig. 3.3 Image of Hydraulic press**

#### **V. Sintering:**

Sintering is a thermal treatment for bonding particles into a coherent, predominantly solid structure via mass transport events that often occur on the atomic scale. The bonding leads to improved strength and lower system energy [16].

The sintering process is divided in two steps one is heating sample at 300°C at 3°C/min rate and maintain for 1 hour in closed furnace for binder burn out. Second heating to 1100°C with 5°C/min rate and maintained it for 4 hours where reduction in surface energy act as driving force to diffuse the particles and densifies the pellet. At high temperature there is high atomic mobility and the bonding of atoms reduces the overall energy of the system. Sintering process is systematically illustrated in fig3.3.

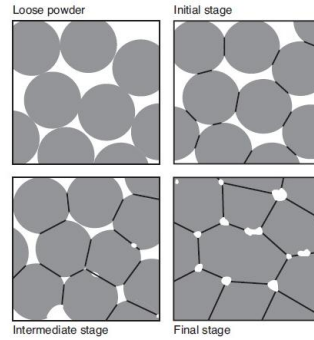


**Fig.3.4: Systematic representation of stages in sintering process [16]**

As the loose powder particle start to react and inter diffuse into each other the porosity decreases. Thus the neck formation signifies strengthening of the material and at final stage there are minimal pores with maximum density. The rate of particle bonding during sintering depends on temperature, materials, particle size and several processing factors. The percentage of weight loss was found to be 1% after sintering process. Fig 3.5 shows the steps involved in sintering process.

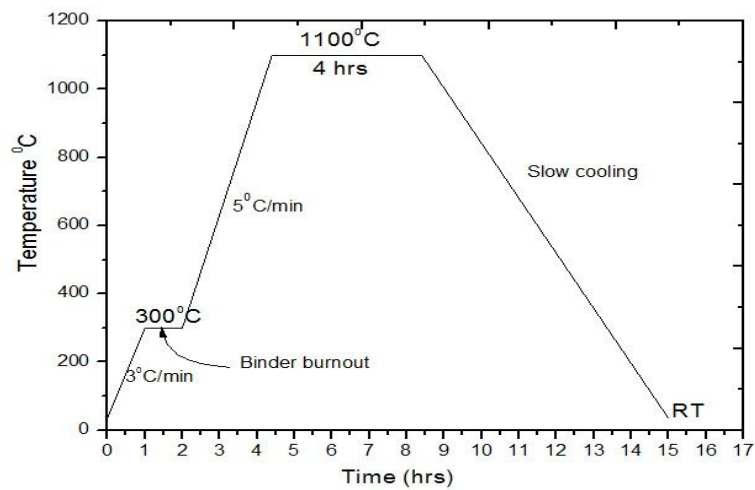


**Fig 3.5: Schematic representing the Sintering cycle**

As the bismuth is volatile compound so that to avoid the deficiency of bismuth, the pellets were covered with NBT powder and the crucible was sealed properly with alumina paste.

SEM micrographs were obtained of just sintered pellet to check the density and to observe the surface morphology. The relative density of sintered sample was calculated by

$$\text{Relative density} = \frac{\text{calculated volume} \times \text{weight of sintered sample}}{\text{Standard density of NBT (5.96 gm/cm}^3\text{)}} \quad \dots\dots 3.1$$

#### **VI. Electroding:**

The sample surfaces were polished for smoothness by 800, 1200 and 1500 grit emery papers and then silver paint was utilized as an electrode. The painted samples were kept in the oven at 100°C for 2 hours to for curing the silver paint. For the accuracy and the quality of characterization results depends on the electroding. As it should be perfectly adhere to the surface and should have minimum resistance and layer should be thin. The other sample was coated with gold of 3nm thickness for SEM analysis by sputtering instrument Quorum (QT150T S) show in Fig. 3.6



**Fig 3.6: Image of Sputter coater**

#### **VII. Electrical Poling**

The poling process which in material is heated and simultaneously large electric field is applied to align the randomly oriented dipoles in domains along the field then for maintaining this condition for some time it is cooled slowly keeping the field constant. So the NBT electrode pellet was kept in crucible containing silicone oil. Silicone oil was used to avoid any sparking at the contacts. A heater kept below crucible heated the sample to 200°C and the field was increased depending on the sample thickness.

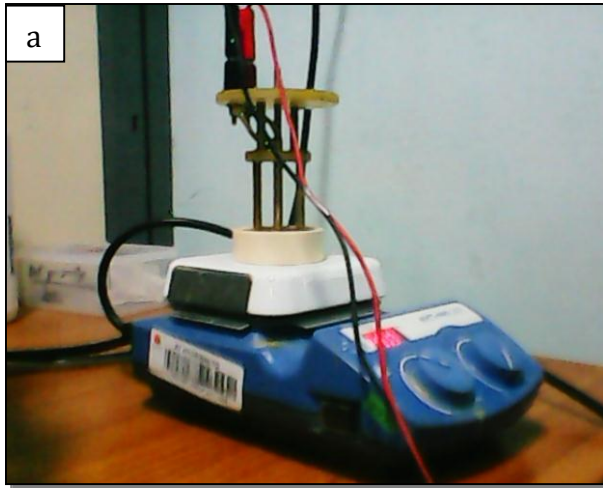


**Fig. 3.7: Setup for poling a) Electrodes, Crucible, Heater b) DC field supply monitoring unit.**

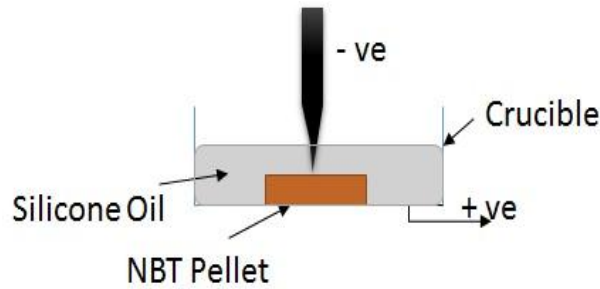


**Fig.3.8: schematic diagram of poling setup**

The Fig. 3.8 explains the complete setup for the poling process. The heating and applying the field was systematically done in step wise manner. The sample was heated gradually increased by  $50^{\circ}\text{C}$  for every 10 to 15 min. similarly the field was increased by  $\sim 250\text{V}$  for every 10 min. finally at highest temperature and voltage it was kept for 15min. and then cooled slowly to room temperature by keeping the voltage constant at highest point. After cooling the remnant polarization in material shows the piezoelectric properties. The details of thickness and applied field are given below.

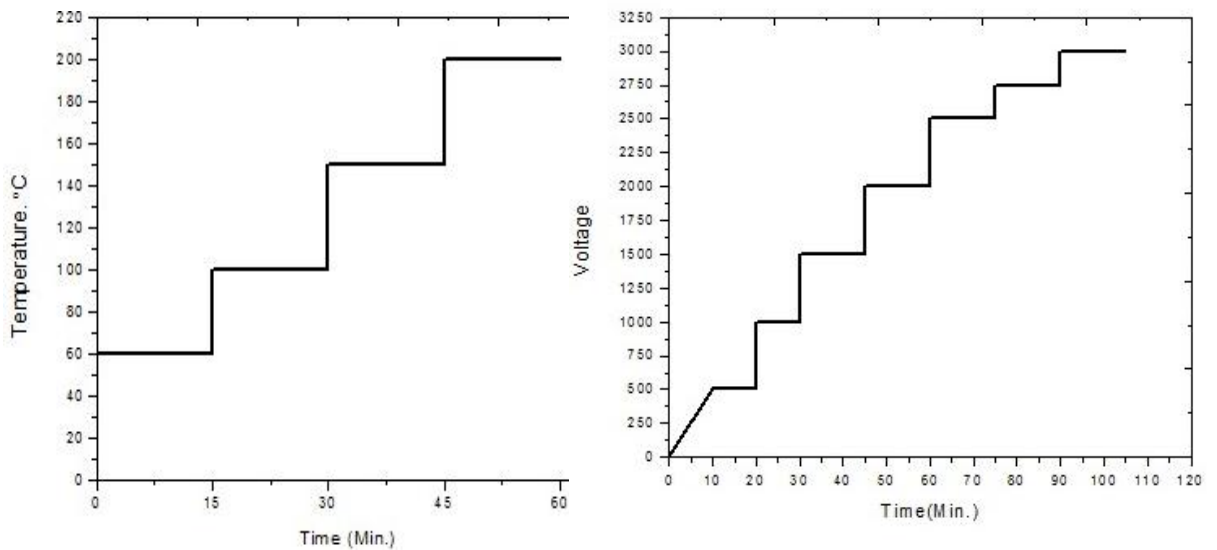


**Fig 3.9: a) Heating cycle for poling process b) Voltage cycle for poling process**



**Table 3.1 Details of NBT pellets used for poling**

	Thickness (mm)	Diameter (mm)	Relative density	Field applied kV/cm at 200°C
<b>NBT Pellet 1</b>	1.43	7.19	~94%	20.9
<b>NBT Pellet 2</b>	0.5	7.19	~94%	74

### 3.2 Synthesis of PVDF thick films

As the work of the project aim for synthesis of a free standing thick film of PVDF/NBT composite for piezoelectric application. At first the PVDF films are prepared by solution casting technique for characterization of  $\beta$ -phase in PVDF. This method gives control on operating parameters such as temperature, solvent, annealing condition which prominently controls the crystallinity in PVDF [36]. Solution casting is a technique in which polymer powder is mixed thoroughly with polar solvent till it becomes a viscous/gel like solution. Then the solution is spread over glass substrate or aluminum foil by a blade and kept in vacuum furnace for baking at some low temperature for some hours.

Following is the systematic flow chart of PVDF film Synthesis.

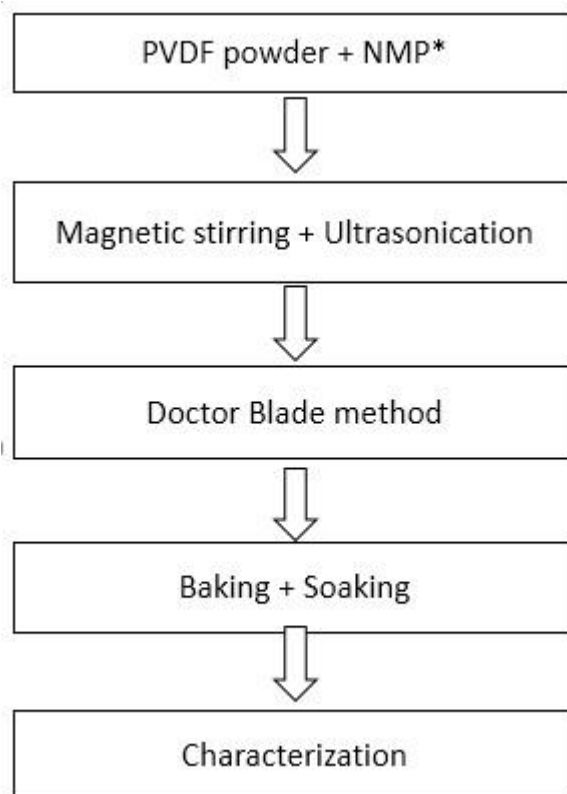


**Fig.3.5 Flow chart of PVDF synthesis and characterization**

## **I. Mixing of precursors**

PVDF (Sigma Aldrich) powder and NMP (Sigma Aldrich) solvent with proper weight proportion was mixed. Example 150mg of PVDF powder was mixed with 1ml of NMP and with requirement few drops of NMP was added in solution. The solution was then mixed by magnetic stirring and ultrasonication 15min each simultaneously for 90min. gradually it forms a dense gel like mixture.

## **II. Deposition**

The thick viscous solution after mixing was then spread on Al-foil by Doctor Blade technique. The Doctor Blade method has a vacuum bed which holds the Al foil tightly and the metallic blade with screw gauge sets the thickness and spread the solution uniformly onto the Al foil.

## **III. Baking**

After spreading the solution on the Al foil, the solution was kept in vacuum oven at 60°C for 8 hrs. While baking the solvent evaporates and the film is formed. The baked film was then characterized by XRD, Raman Spectroscopy, and SEM for its phase formation.

## **IV. Annealing of Films**

As the  $\beta$ -PVDF is desired phase for piezoelectric application due to its large polarization. But the  $\alpha$ -PVDF is the stable phase found while synthesis at lower temperature. So to analyze the effect of annealing temperature on the phase formation in the film, the film was heated for various temperatures 70, 80, 90, 100, 110, 120 and 130°C. The annealed films were then characterized by XRD, SEM.

## **V. Electroding and poling**

The pure PVDF film was electroded by copper with approximately 400nm thickness. The electroding of copper on PVDF was done by DC Sputtering. The electrode sample was tried for poling under applied electric field. Also gold coating of ~3nm was done to characterize film by SEM.



**Figure 3.6** Picture of the synthesized and electroded NBT ceramic pellets and PVDF thick film

The figure 3.6 given above shows the image of NBT ceramic pellets and PVDF film which was utilized further for structural and electrical characterization.

### 3.3 Synthesis of PVDF/NBT composite films

The synthesis technique of Composite films is almost similar to synthesis of PVDF films.

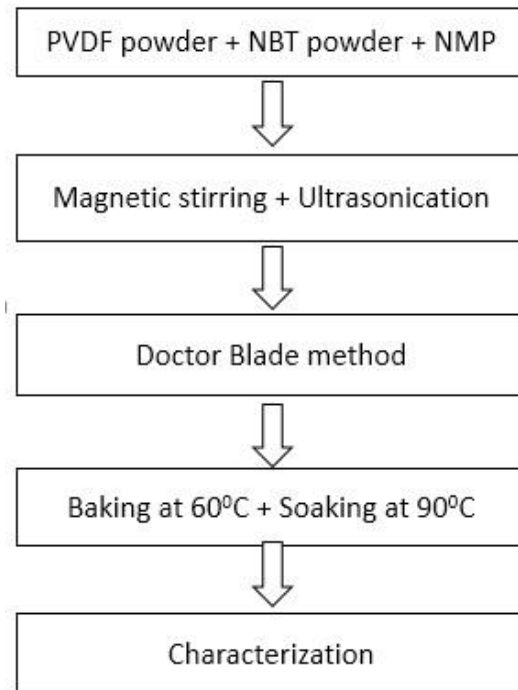


**Fig.3.7: Flow chart for synthesis of PVDF/NBT composite films**

#### I. Mixing of precursors

PVDF (Sigma Aldrich) powder, NMP (Sigma Aldrich) solvent and NBT calcined powder was mixed with proper weight proportion. By keeping the quantity of PVDF and NMP constant in mixture to 150mg and 1ml respectively, the mass of NBT powder was varied to get composite films of various mass percentages. So the composite films with NBT mass percentage of 5, 10, 20, 25, and 30 were prepared. Similar to PVDF film synthesis the all precursors were mixed by magnetic stirring and ultrasonication simultaneously each 15min and total process for around 90min. till the solution becomes highly viscous gel like substance.

#### II. Deposition

The thick viscous solution was then spread on Al-foil by Doctor Blade technique. The Doctor Blade method has a vacuum bed which holds the Al foil tightly and the metallic blade with screw gauge sets the thickness and spread the solution uniformly onto the Al foil.

### **III. Baking and soaking**

After spreading the solution on the Al foil, the solution was kept in vacuum oven at 60°C for 8 hrs. While baking the solvent evaporates and the film is formed. And also the films were soaked for 90°C for 8hrs. The prepared films were then used for characterization.

### **IV. Gold Coating**

To characterize the composite films by SEM to see the dispersion of NBT particle in PVDF matrix. So to avoid charging effect films were coated gold of ~3nm thickness by sputter coater Quorum Q150T S.

## **3.4 Characterization techniques**

The above synthesized materials are characterized by various experimental techniques at different measurement conditions to study its structural and functional properties. The fundamental of characterization techniques used is explained with an example of prepared sample. Various characterization techniques were used depending on the sample material, so systematically characterization of PVDF films, NBT powder and pellets and PVDF/NBT composite films under particular method is described below. The characterization was done by X-Ray Diffraction, Raman spectroscopy, Scanning electron microscopy, impedance spectroscopy, tensile testing, Vibration detection etc.

### **3.4.1 X-ray diffraction**

X-ray diffraction (PANalytical, Xpert Pro) is characterization technique which gives the details atomic arrangements, crystal structure of the material. The X-rays of wavelength ( $\lambda$ ) 1.54Å are incident on the material while the detector collects the constructive interference pattern of diffracted rays coming from the plane which satisfies the Bragg condition. Where  $n$  is the order of diffraction,  $d$  is interplanar distance of crystal and  $\theta$  is angle of incidence. The XRD scan was done at room temperature from  $5^\circ \leq 2\theta \leq 120^\circ$  value with time of 30min for each scan.

The XRD was done for following sample to verify and study the phase formed in material after the reactions

1. XRD of PVDF films annealed and different temperatures
2. XRD of NBT calcined powder
3. XRD of NBT sintered pellets
4. XRD of PVDFNBT composite films

### **3.4.2 Scanning electron microscopy**

The scanning electron microscope (Carl Zeiss Supra 40) was used for obtaining high resolution micrographs of NBT pellets, PVDF film, and Composite films. The micrographs used to study the morphology and the crystal structure of the material.

Secondary electrons and backscattered electrons are used for imaging samples. Secondary electrons gives morphology and topography of samples and backscattered electron illustrate the contrasts in composition in multiphase samples.

### 3.4.3 Dielectric studies

The dielectric study includes the analyzing the graphs of frequency dependent dielectric constant vs. temperature plot, P-E Hysteresis loop, calculating the resonance frequency, dielectric loss and phase transformation in material. The sample were electroded NBT pellets, and PVDF film

The dielectric measurement was done by following instruments

- i. Wayne KERR Impedance analyzer: To study Frequency dependent Dielectric constant vs. Temperature graph



**Fig 3.8 Image of Wayne KERR (6500B) Impedance analyzer**

- ii. Precision Impedance analyzer (Agilent 4294A) operates in range of 40Hz to 110MHz: To analyze the resonance frequencies of a material.



**Fig 3.9: Image of Agilent (4294A) Precision Impedance analyzer**

iii. P-E hysteresis measuring instrument

The results from Ferroelectric Loop tracer (aixACT) were used to calculate remnant polarization and coercive field of a given material

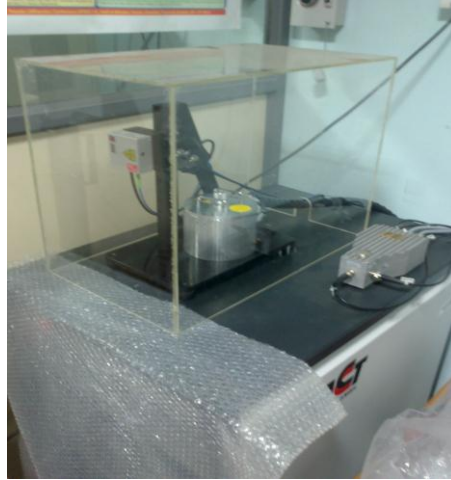


**Fig. 3.11: P-E hysteresis loop tracer**

iv. Piezometer System PM300 : To calculate  $d_{33}$  coefficient of material



**Fig.3.12 Piezometer system setup for  $d_{33}$  measurement**

The principle of operation of this instrument is quite simple as it applies low frequency force on electroded sample which generates electrical signals which is compared with built in reference and gives  $d_{33}$  coefficient value. The dynamic force was kept to 0.25N and frequency to 110 Hz for measuring  $d_{33}$  for NBT samples.

#### **3.4.4 Raman Spectroscopy**

Vibrational spectroscopy is extensively used to study the structure, physical and chemical properties of crystal structure and molecule. Raman spectroscopy technique is used to study the detailed molecular structure. It works on the principle of polarizability. The Raman spectrometer (SENTERRA) was used to study the characteristic vibration modes in PVDF and NBT. Operating parameters such as laser power was varied 5mW to 25mW and two different wavelengths were used 532nm and 785nm.

### **3.4.5 Mechanical behavior of Composite and PVDF thick films**

MTS Instron 3367 with Bluehill 2.0 software with load cell was of 500N capacity was used to study the elastic behavior of PVDF film as well as PVDF/NBT composite films. The rate extension was 1mm/min and tensile loading. The load vs. deflection graphs were plotted to study the effect of change in mass percentage of NBT particle in composite film.

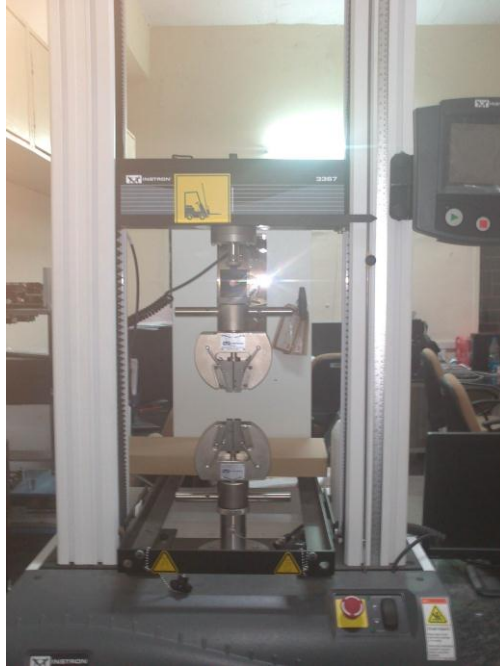


**Fig. 3.12: Image of Instron MTS used for tensile testing**

# Chapter 4

## Results and Discussion

This chapter deals with the results obtained from the structural and physical property studies performed on  $\text{Na}_{0.5}\text{Bi}_{0.5}\text{TiO}_3$  (NBT) ceramics, PVDF polymer and NBT-PVDF composite. The chapter initially deals with results obtained from NBT ceramics followed by PVDF and NBT-PVDF composite.

### 4.1 Results and discussion on NBT ceramic

The structural studies on NBT ceramics was done by X-Ray diffraction utilizing powder diffractometer, Raman spectroscopy, and the microstructural studies was done by scanning electron microscopy.

#### 4.1.1 Structural analysis of NBT

The NBT ceramics synthesized through solid state reaction route was characterized using x-ray diffraction studies in a powder diffractometer operating in a  $\theta$ - $2\theta$  geometry. The diffraction pattern was utilized to confirm the phase formation of the compound upon solid state reaction. The Fig 4.1 shows the XRD pattern for NBT powder calcined at  $850^\circ\text{C}$ . The pattern confirms the formation of phase pure crystalline compound as it exhibits sharp peaks and the peak positions matching with earlier reported data available in the crystallographic database [14]. The d spacing for every diffracted miller indices is tabulated in table 4.1

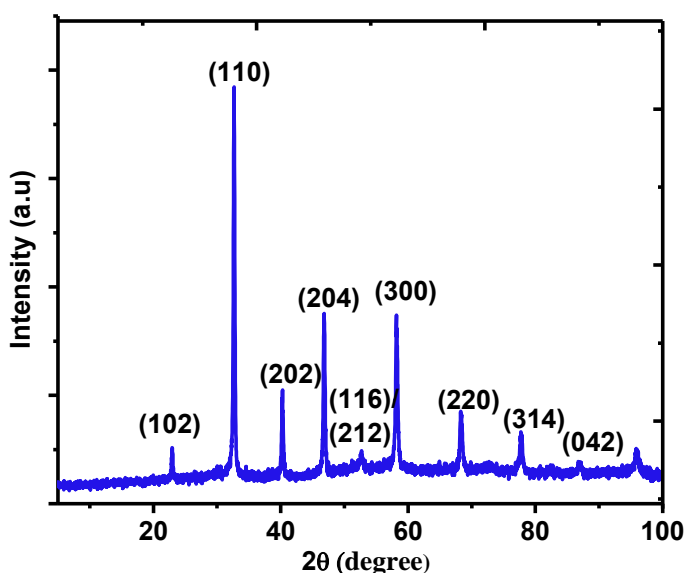


Fig 4.1 Powder diffraction pattern of calcined NBT powder



**Table 4.1 Details of calculated d spacing related to particular miller indices for NBT**

$2\theta$	d spacing (Å)	Miller Indices		
		H	K	L
22.9393	3.8768	1	0	2
32.6633	2.7414	1	1	0
40.2793	2.2389	2	0	2
46.8073	1.9400	2	0	4
52.6893	1.7371	2	1	2
58.1433	1.5865	3	0	0
68.3469	1.3724	2	2	0
77.8663	1.2267	3	1	4
87.1653	1.1182	0	4	2

The reported values of lattice parameters for this graph is  $a = 5.488\text{Å}$ ,  $c = 13.538\text{Å}$  which is rhombohedral structure at room temperature.

Initially to check the effect of calcination temperature on phase formation the precursors were calcined at three different temperatures  $750^{\circ}\text{C}$ ,  $800^{\circ}\text{C}$  and  $850^{\circ}\text{C}$ . Fig 4.2 shows the observed difference in phase formation in XRD.

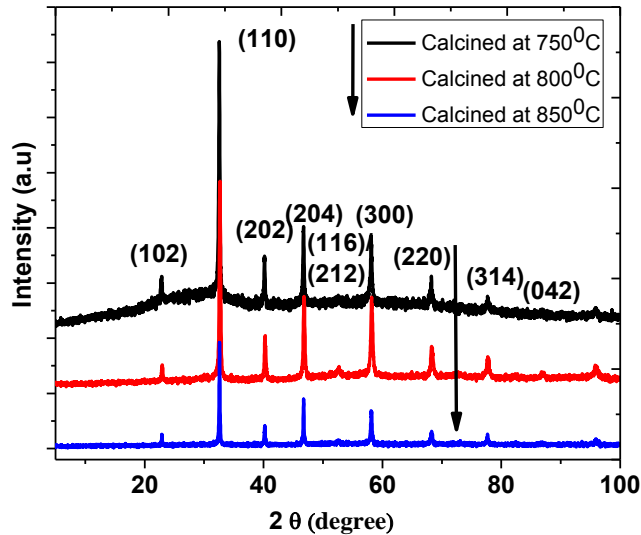


**Fig. 4.2 XRD of NBT powder calcined at different temperatures**

The powders calcined at  $850^{\circ}\text{C}$  resulted in the formation of phase pure NBT ceramic powders. The room temperature, crystal structure is commonly observed to be rhombohedral, however, structural studies performed from a local regions suggests possibility of mixed phases in NBT at nano scale and also remains ambiguous.[37,38] In addition to XRD analysis Raman spectroscopy was done to get the details about the vibrational modes present.

The Raman spectra shown in Fig. 4.3 shows various Active Raman modes observed for NBT. The major modes observed in NBT are at 138, 272.2, 530, 585, 770 and 830  $\text{cm}^{-1}$ .

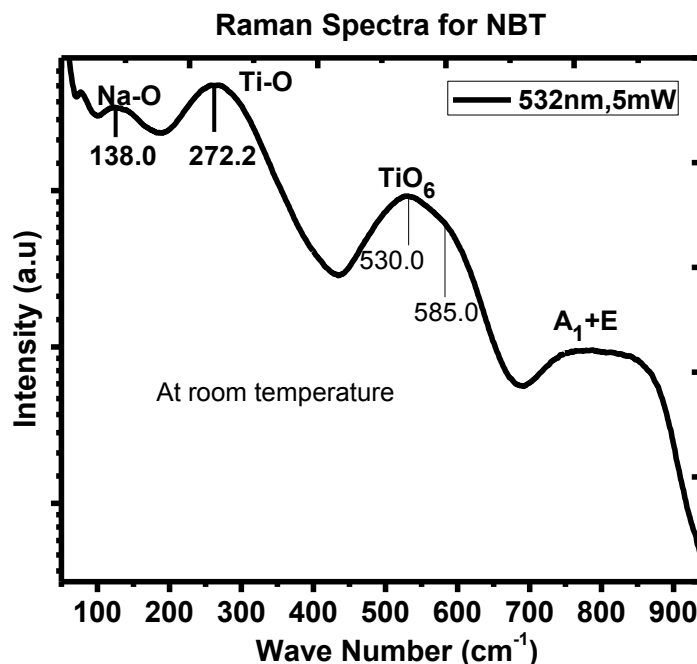


**Fig 4.3: Figure shows active Raman modes present in NBT**

The first low frequency band observed at 138  $\text{cm}^{-1}$  is associated with the Na–O bonds, whereas 280 is A<sub>1</sub> mode associated to Ti-O bond. The vibrations of TiO<sub>6</sub> octahedron gives bands at higher frequencies 530 and 580  $\text{cm}^{-1}$  and confirms the formation of perovskite structure, this bands are due to superposition of transverse optical (TO) and longitudinal optical (LO) bands of A<sub>1</sub> character. The oxygen vacancies present in pure NBT gives rise to band at 770 & 830  $\text{cm}^{-1}$  that are linked to A<sub>1</sub> (LO) and E (LO) overlapping bands. The reason of oxygen vacancies is due to volatility of Bismuth during sintering. The broadening in bands due to disorder at A-site of NBT is explained by B K Barick et al (2011) [14]. The Bi-O bond is not observed at lower frequencies because of higher mass of bismuth atom.

#### 4.1.2 Morphological studies of NBT by SEM

The synthesized NBT powders were sintered at 1100°C for 4 hours in a sealed high pure alumina crucible. The microstructural and surface morphological studies of the sintered ceramic pellets were carried out using SEM. The SEM micrograph of sintered pellet of Na<sub>0.5</sub>Bi<sub>0.5</sub>TiO<sub>3</sub> is shown in Fig.4.4 shows the extensive polycrystalline microstructure with nearly rectangular grains of different grain sizes and they are in-homogeneously distributed throughout the sample surface. The grains and grain boundaries are well defined, the necking occurred in sintering process is clearly visible.

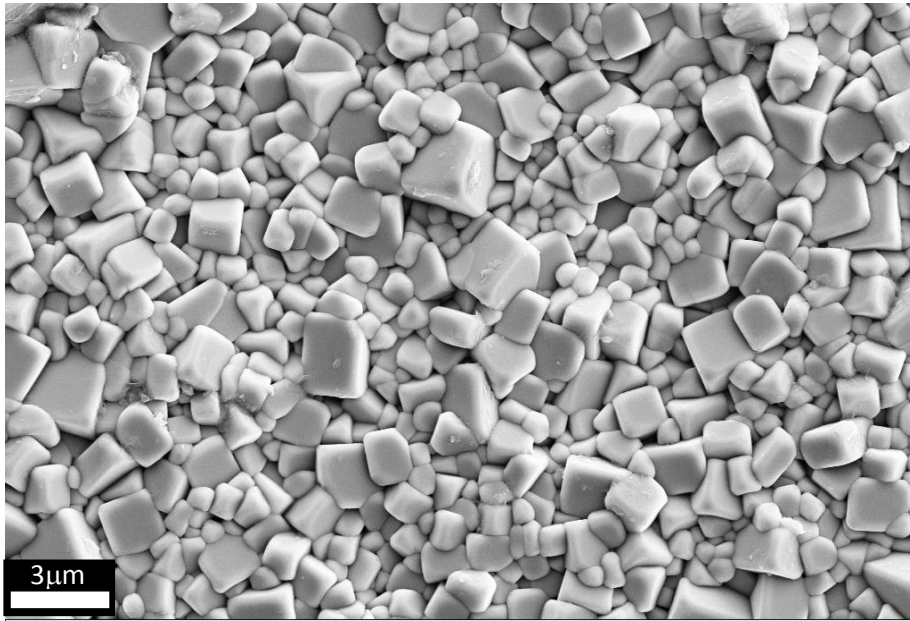


**Fig.4.4: SEM micrograph of NBT (magnification 10kX)**

The microstructure is overall dense, but a few scattered pores could be observed which could have arisen due to polishing. The average grain size lies between 1 to 3  $\mu\text{m}$ .

#### 4.1.3 Physical property studies on NBT

Furthermore the sintered dense NBT pellets were utilized to study the physical properties such as dielectric behavior, phase transformation, hysteresis loop,  $d_{33}$  coefficient etc.

The dielectric measurements were done using an Impedance analyzer (Agilent, 4294A), P-E loop tracer, Piezotest and the electrical parameters such as parallel capacitance ( $C_p$ ), and dielectric loss ( $D$  or  $\text{Tan}\delta$ ) were recorded to plot the results .

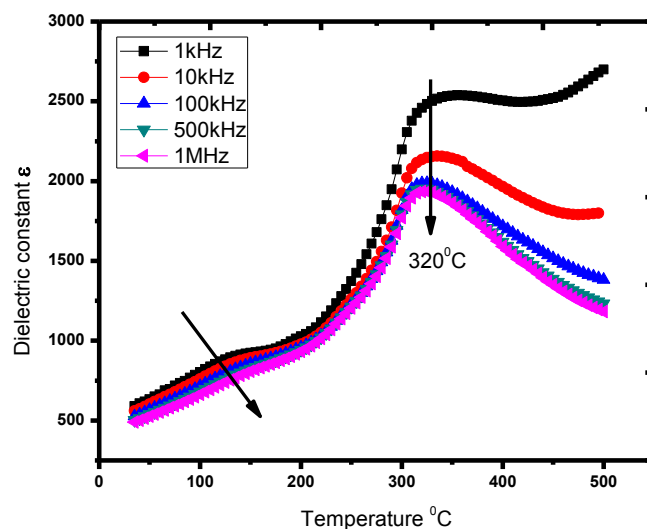


**Fig.4.5: Dielectric constant with respect to temperature at different frequencies**

The graph shown in Fig. 4.5 explains about variation of dielectric constant with temperature at the few selected frequencies. It is observed that the dielectric constant increases with increase in temperature to its maximum value ( $\epsilon_{\max}$ ) and then decreases. The dielectric anomaly is observed around 320 °C representing the antiferroelectric - paraelectric phase transition. The peak in the pattern appears at the same temperature irrespective of the frequency. It is also observed that around the temperature 200°C there is a bifurcation in dielectric constants for different frequencies, which may be due to the ferroelectric to anti-ferroelectric phase transition of NBT. Further, this phase transitions also involves structural phase transformations such as at 200°C it transforms from rhombohedral (ferroelectric) to tetragonal (anti-ferroelectric) phase transformation, and at 320°C there is tetragonal (anti-ferroelectric) to cubic (paraelectric) phase transformation. The dielectric constant at low frequency observed to be increased with the increase in temperature above phase transition temperature, which may be due to space charge polarization and its conductivity. The observed dielectric constant for NBT is **1935.0** at 1MHz. The decrease in dielectric constant with increase in frequency signifies normal behavior of polar dielectric.

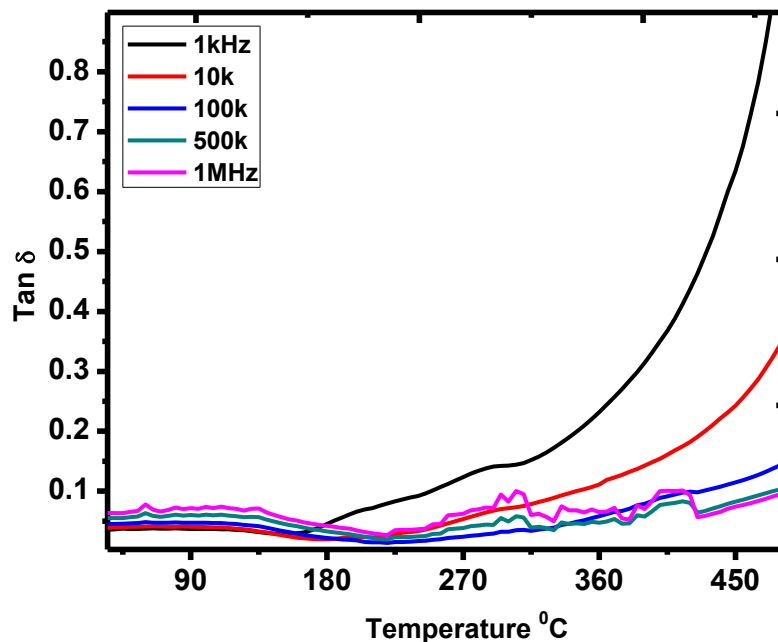


**Fig.4.6: Dielectric loss with respect to temperature at different frequencies**

The variation of  $\tan(\delta)$  with the temperature at different frequencies of NBT is shown in Fig. 4.6. It is observed that the tangent loss increases with increase in temperature at all frequencies except the depression observed near 200° C. The depression can be due to anti-ferroelectric to ferroelectric phase transition as similar to this temperature hump is observed in dielectric constant vs. temperature graph shown in Fig. 4.6. It is observed that the dielectric losses are low and are constant up to 100°C. The observed value is **0.07** at 1MHz frequency at room temperature.

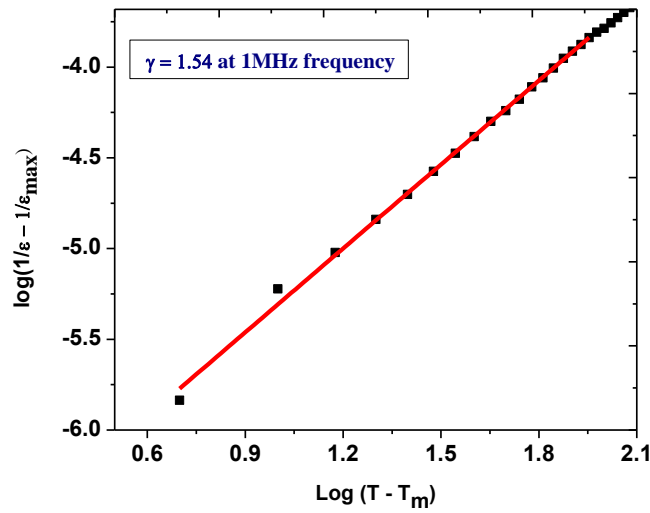


Fig.4.7: Modified Curie – Weiss law

In addition there is a broad transition observed for NBT at the Curie temperature, which is expected to arise due to the plausible structural heterogeneity present between the rhombohedral and the tetragonal phase. Hence, a modified Curie-Weiss plot was utilized to characterize the diffusiveness of the phase transformation. The diffusivity ( $\gamma$ ) is calculated from the slope by using modified Curie-Weiss law as given in equation 4.1.

$$\left(\frac{1}{\epsilon} - \frac{1}{\epsilon_m}\right) = (T - T_m)^{\gamma} / C \quad 4.1$$

The value of diffusivity ( $\gamma$ ) is 1.54 at 1MHz, which proves that the phase transition in NBT is a diffuse phase transition. The corresponding plot is shown in figure 4.7. To analyze the important physical properties for NBT such as its coercive field, remnant polarization P-E hysteresis loop was measured by ferroelectric loop tracer at room temperature.

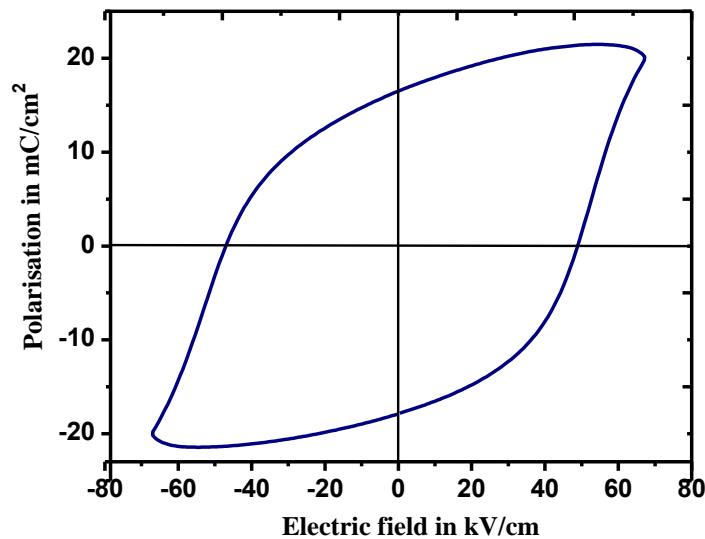


Fig.4.8: P-E Hysteresis Loop for NBT

The P-E loop shown in Fig.4.8 shows a typical hysteresis behavior of ferroelectric material. From the P-E loop it is observed that the remnant polarization ( $P_r$ ) for NBT is **16.47  $\mu\text{C}/\text{cm}^2$**  and coercive field ( $E_c$ ) is **47.19kV/cm** at 1 Hz frequency. It was also observed that the sample was leaky as at the saturation point it shows smooth curvature instead of sharp point. The recorded coercive field from hysteresis loop is comparatively larger than the conventional piezoelectric materials.

Though it exhibits a strong ferroelectric character with larger coercive fields it hinders while poling the material. The important parameters needed for designing any piezoelectric material for any practical application is its piezoelectric coefficients.

Piezoelectric constant  $d_{33}$  is calculated for three different NBT pellets which were poled at different poling fields. The results are tabulated in table 4.2. The samples tested are unpoled, poled at 20.9kV/cm and poled at 74kV/cm. the relation between  $d_{33}$  and  $g_{33}$  is

$$g_{33} = \frac{d_{33}}{\epsilon \times \epsilon_0}$$

Where  $\epsilon$  is dielectric constant and  $\epsilon_0$  is permittivity of free space ( $8.9 \times 10^{-12} \text{F/m}$ )

**Table 4.2 Results of Piezoelectric coefficients for NBT samples**

	$d_{33}$	$g_{33}$
Unpoled	0	0
Poled 20.9kV/cm	<b>16<math>\rho\text{C}/\text{N}</math></b>	<b>0.93<math>\times 10^{-3} \text{Vm}/\text{N}</math></b>
Poled 74kV/cm	<b>74<math>\rho\text{C}/\text{N}</math></b>	<b>4.30<math>\times 10^{-3} \text{Vm}/\text{N}</math></b>

From the calculated values of piezoelectric coefficients it is clear that the poled sample at higher electric field gives larger  $d_{33}$  and  $g_{33}$  this values are quite competitive with the results already reported by the researchers [3, 5,15].

The physical property which will tell about the practicality of using these materials is understood from its coupling coefficient and the resonance frequencies. This analysis was done by the results of Cp-D plots. The samples tested are unpoled NBT sample and poled NBT samples with different poling fields with also different thicknesses.

#### Details of samples

1. Poled sample at 20.9kV/cm thickness 1.43mm
2. Poled sample at 74kV/cm , thickness 0.5mm
3. Unpoled sample thickness 1mm

Following is the graph which shows the frequency response of applied electric field on material.

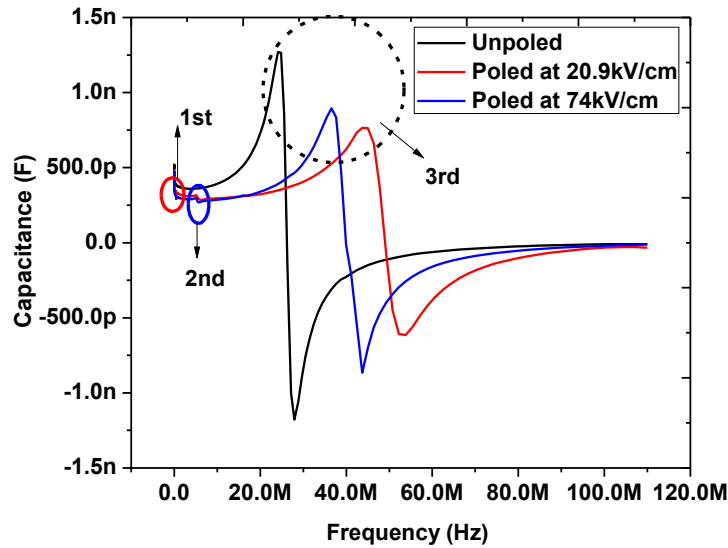


**Fig. 4.9 Combined resonance frequency response of unpoled and two poled sample at different fields of 209 kV/cm and 74kV/cm**

The plotted Cp-D curves in Figures 9- 13 are the result obtain from Impedance analyser. The Cp-D plot gives maximum capacitance for zero impedance which is called as minimum impedance frequency or series resonance frequency and anti resonance occurs at maximum impedance and as capacitance is inversely related to impedance the capacitance will be minimum thus this frequency is called as anti resonance frequency or parallel resonance frequency. The actual resonance frequency of material lies in between this two  $f_m$  and  $f_n$  value.

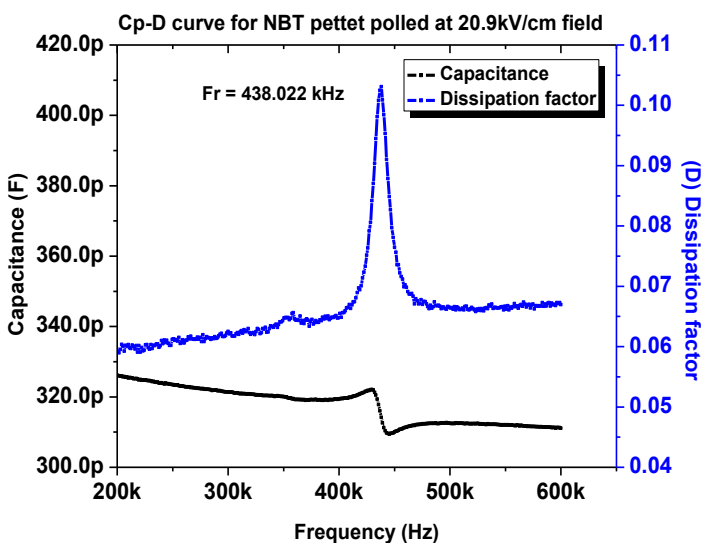


**Fig.4.10 First resonance mode for a sample 20.9kV/cm**

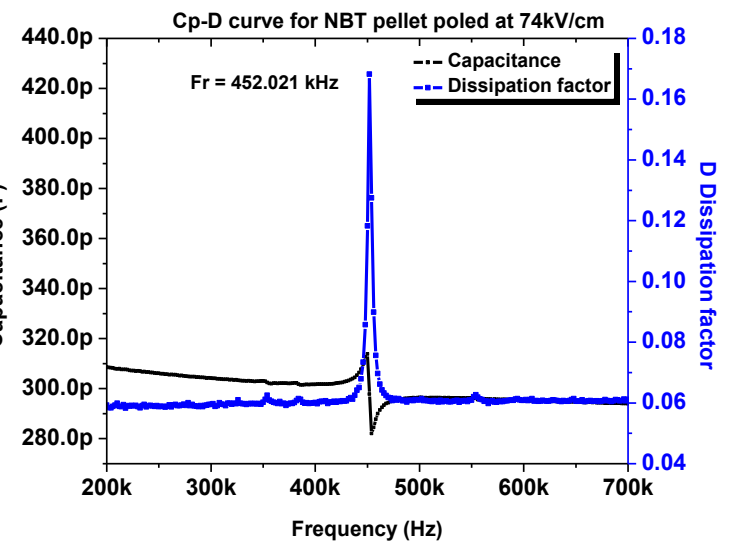


**Fig.4.11 First resonance mode for a sample Poled to Poled to 74kV/cm**

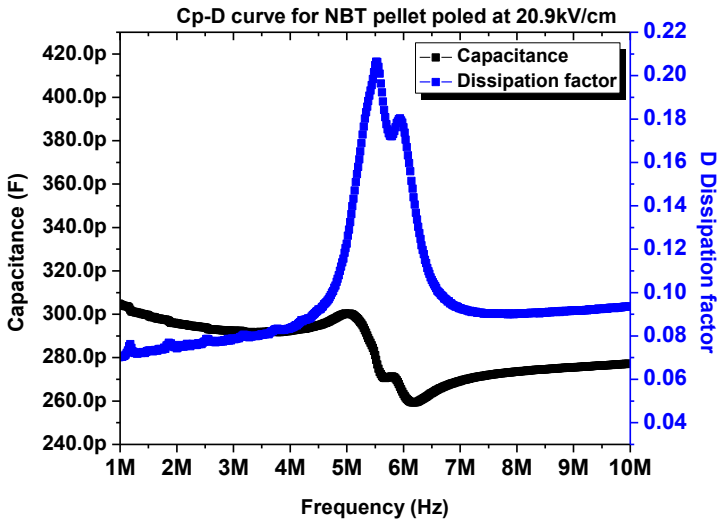


Fig.4.12 First resonance mode for a sample Poled to 20.9kV/cm

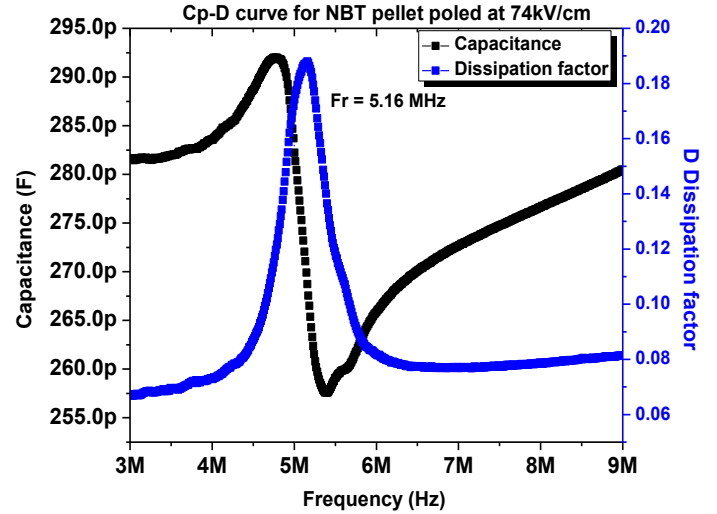


Fig.4.13 First resonance mode for a Poled to 74kV/cm

The resonance frequencies also tells about the coupling of electrical and mechanical energy, hence a sensor operating at or near to the resonance frequency will give maximum efficiency. The efficiency of piezoelectric devices is expressed in terms of coupling constant thus the series and parallel resonance frequencies are related to coupling constant. So the coupling constant and the resonance frequencies are calculated from the graphs. It was noted that there is a difference in response for poled and unpoled sample.

The poled sample shows three different modes where resonance have occurred while 1<sup>st</sup> and 2<sup>nd</sup> mode was absent in unpoled sample of NBT. In fig.4. 9 it is indicated by the circles drawn on the perticular curve location. The first mode of resonance frequency for poled samples was magnified in fig.4.10 and 4.11 . while the 2<sup>nd</sup> mode for both the samples were plotted and have shown some anamoly which can be from electrode material. And the 3<sup>rd</sup> large resonance was noted in all the three samples with different resonance frequencies. The calculated resonance frequencies and coupling coefficients is tabulated in table 4.



**Table 4. 1 Results of resonance frequencies and coupling coefficients for NBT samples**

		Unpoled	Poled at 20.9kV/cm	Poled at 74 kV/cm
Resonance Frequency	1 <sup>st</sup>	N/A	438.022 kHz	452.021 kHz
	2 <sup>nd</sup>	N/A	----	5.16MHz
	3 <sup>rd</sup>	26.34 MHz	49.234 MHz	37.82 MHz
Coupling Coefficient ( $k_p$ )	1 <sup>st</sup>	----	0.315	0.148
	2 <sup>nd</sup>	----	0.656	0.520
	3 <sup>rd</sup>	0.573	0.623	0.616

From the results of coupling constants it can be proved that the efficiency of operation of this material at lower frequencies i.e. below 1MHz is very low compared to higher frequencies.

## 4.2 Results and discussion of PVDF polymer and PVDF/NBT composite

The structural and morphological studies for PVDF film and PVDF/NBT composite films were done by X ray diffraction, Raman spectroscopy and by scanning electron microscopy.

### 4.2.1 Structural studies on PVDF and PVDF/NBT composite

The PVDF films synthesized through doctor blade technique was used for XRD analysis to verify the  $\beta$ -PVDF phase formation. The observed results of XRD for PVDF films annealed at different temperature shows that the film which was annealed at 60<sup>0</sup> have dominant  $\alpha$ -PVDF phase. The characteristic 2-theta value for  $\alpha$ - phase in the XRD pattern is at 18.4<sup>0</sup>, 27.8<sup>0</sup> and for  $\beta$ - phase it is 20.8<sup>0</sup>, 20.7<sup>0</sup>. With increase in annealing temperature the  $\alpha$ -Phase (18.4<sup>0</sup>) decrease and the  $\beta$  PVDF phase formation around 90<sup>0</sup>C. The further increase in temperature shows re-entrance of  $\alpha$  PVDF phase at 27.8<sup>0</sup>. Another study by XRD was done on NBT powder to check the effect of annealing on phase formation but the result have shown that there was no effect on powder as both alpha and beta phase PVDF diffraction peaks are present in all samples

The Fig 4.14 a) show the XRD graph of annealing of PVDF films and Fig 4.14 b) shows the XRD graph of raw PVDF powder annealed at different temperature.

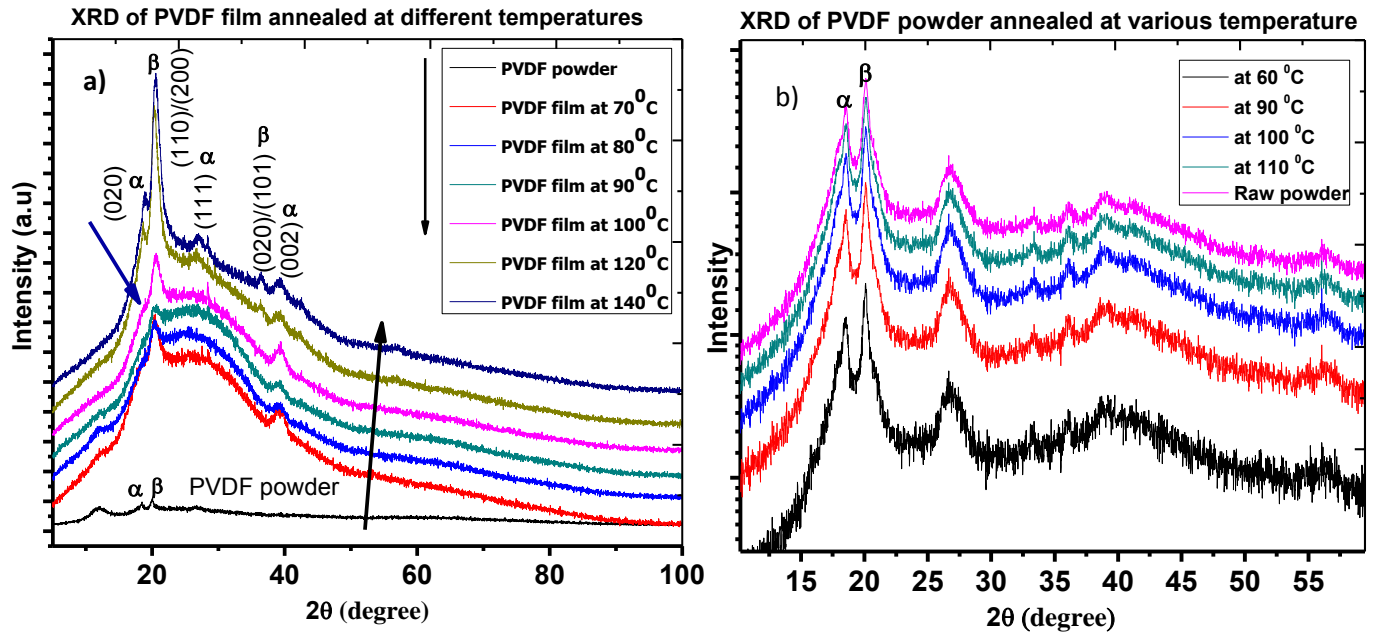


Fig.4.14: a) Fig. XRD graph of PVDF film annealed at different temperatures. b) XRD graph of PVDF powder annealed at different temperatures

- **Mechanism of  $\beta$ - phase formation from solution :**

The high polar solvent like DMSO (Dimethyl sulfoxide), DMF (Dimethyl formamide), NMP (N-Methyl-2-pyrrolidone) tends to rotate the strong dipoles of C-F bond in PVDF molecular chain. Single polar solvent can produce different phase in PVDF depending on preparation temperature. At temperature below 50°C the viscosity of PVDF solution is high and low thermal energy is not sufficient to rotate the polar groups. So  $\alpha$ -PVDF is formed with no *trans* – *gauch* conformer. When the PVDF is prepared at 90°C the viscosity of solution is low and thermal energy is sufficient to rotate the CF<sub>2</sub> polar group forming  $\beta$ - PVDF is formed with large *trans*- *gauch* conformational change to TTTT form [36].

To analyze the coexistence of NBT and PVDF phases in a single composite XRD technique was used. The composite was a particulate composite as NBT particles embedded in polymer matrix. The PVDF/NBT films of varying weight percentage as 5%, 10%, 20%, 25%, and 30% were characterized by this technique and the results are given below.

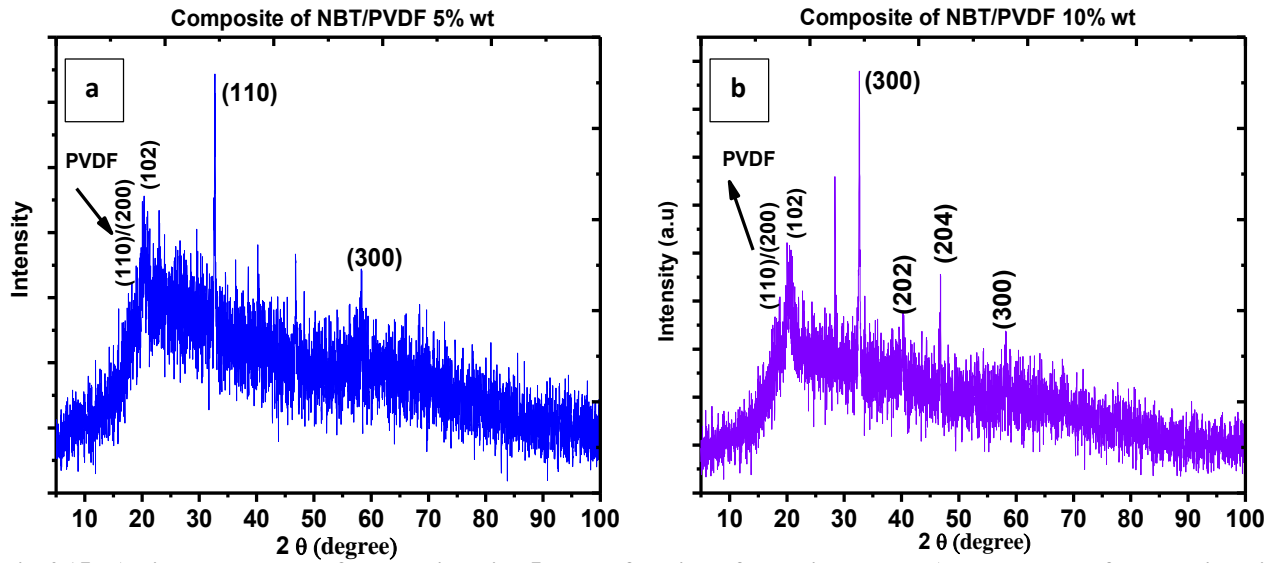


Fig.4.15: a) Fig. XRD result of composite with 5 % wt. fraction of NBT in PVDF. b) XRD result of composite with

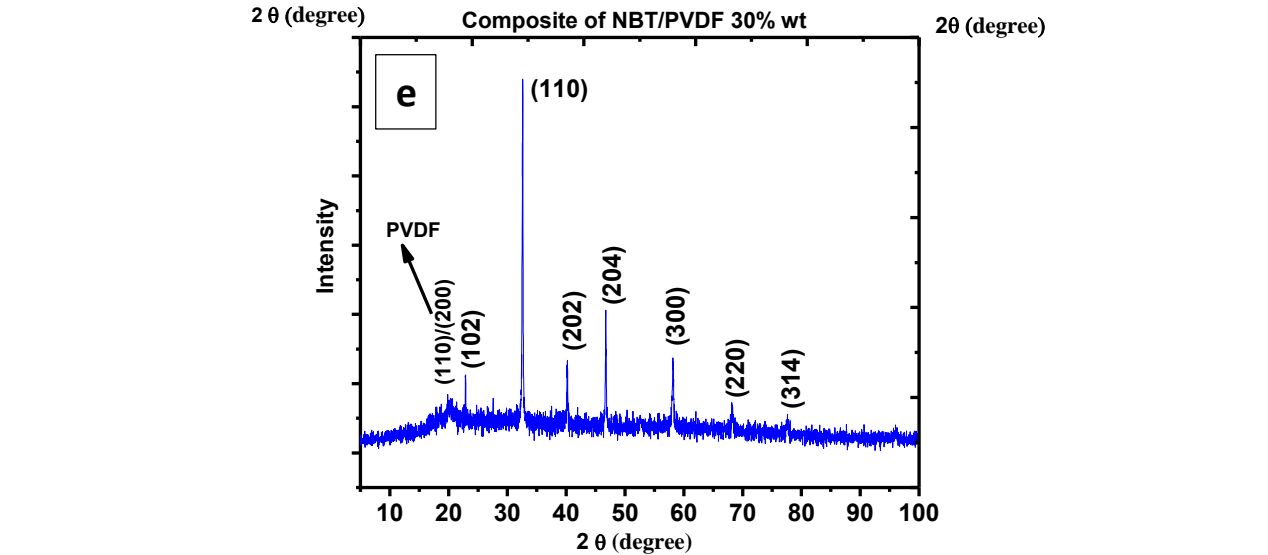
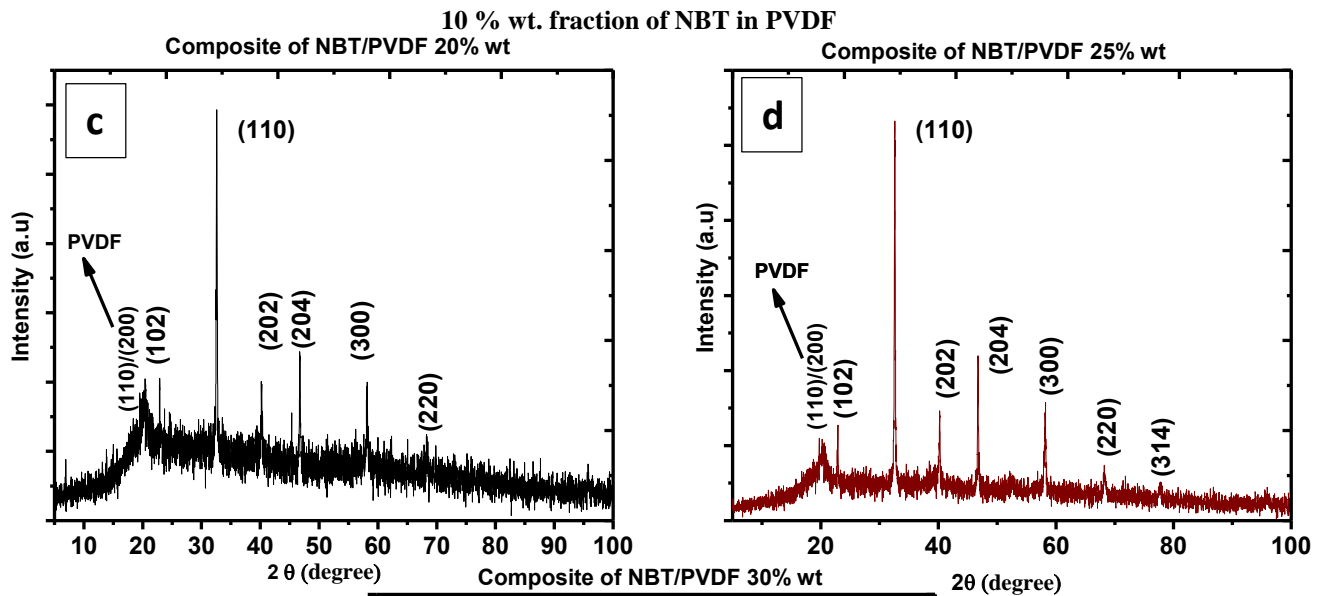
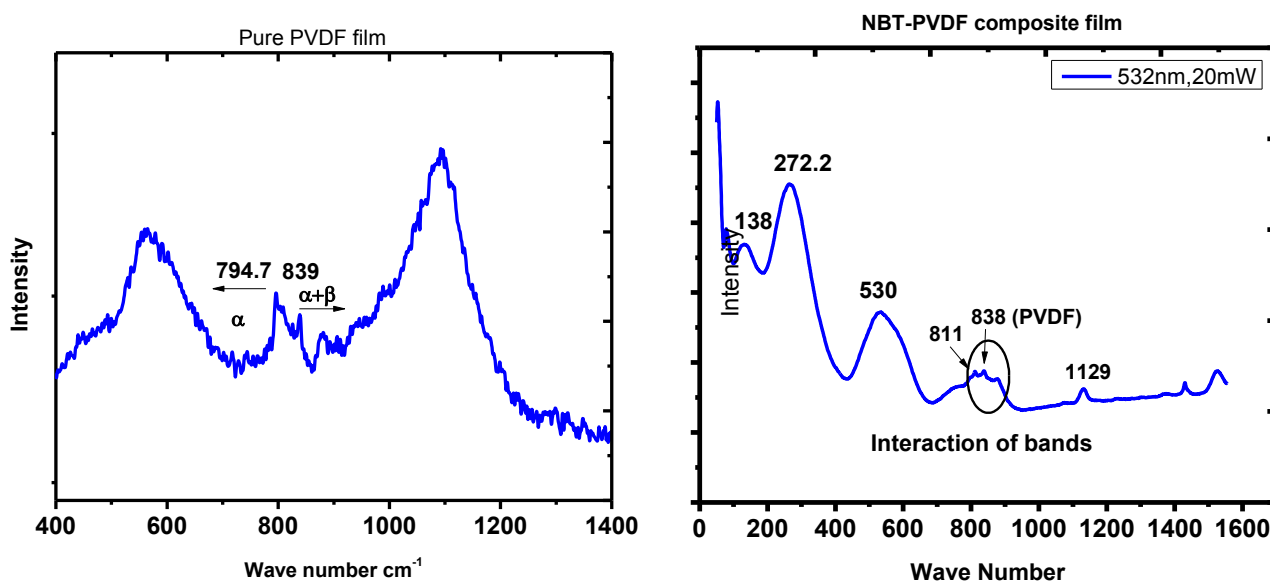


Fig.4.16: c) Fig. XRD result of composite with 20 % wt. fraction of NBT in PVDF. d) XRD result of composite with 25 % wt. fraction of NBT in PVDF. e) XRD result of composite with 30 % wt. fraction of NBT in PVDF

The XRD pattern of 5%PVDF/NBT composite in Fig. 4.15 a) clearly shows the dominance of PVDF presence in the compound due to presence of a characteristic peak of PVDF at  $20^\circ$  for (110) and (200). The broaden peaks throughout the curve tells about the semi-crystallinity of material. NBT peaks are totally suppressed showing very less intensity. Gradually from the figure b), c), d), e) it is observed that as the mass percentage of NBT particles increase in PVDF matrix the overall crystallinity of composite increases. The characteristic peaks of NBT get intense with the increase in mass percentage but there are some peaks present related to PVDF. Thus it can be concluded that there is no formation of new compound in composite and both the elements are individually contributing in formation of particulate composite where ceramic particles are dispersed in polymer matrix.

The modes of vibrations related to PVDF and NBT PVDF composite was studied by Raman spectroscopy. The main aim was to confirm the phase formed in the material.



**Fig. 4.17: a) Results of Raman Spectroscopy for pure PVDF film b) Results of Raman spectroscopy for PVDF/NBT film.**

The band at  $794.7 \text{ cm}^{-1}$  signifies the presence of  $\alpha$ -PVDF. The band at  $839 \text{ cm}^{-1}$  signifies the presence of mixed  $\alpha + \beta$  PVDF phase. Results shows the coupling of NBT and PVDF Raman bands between  $780$  to  $880 \text{ cm}^{-1}$ .

#### 4.2.2 Morphological studies of PVDF and PVDF/NBT composite films by SEM

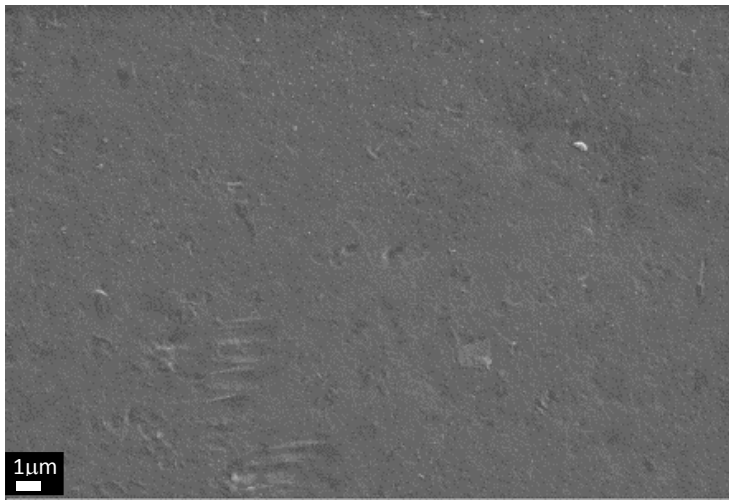


Fig.4.18: PVDF film (magnification 10kX)

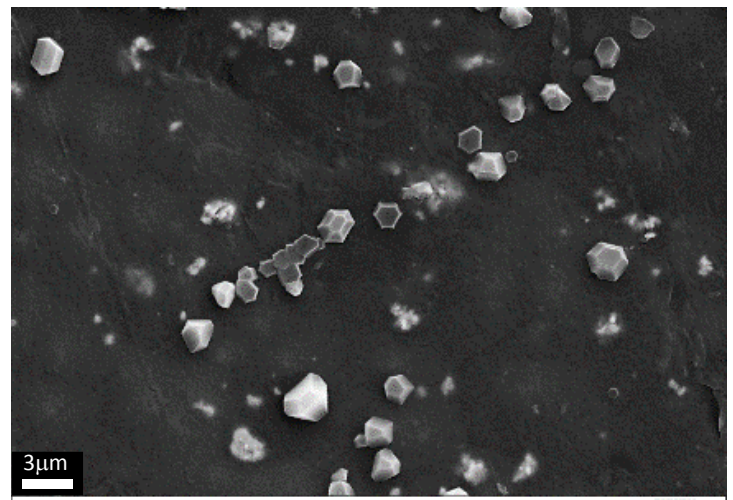


Fig.4.19: PVDF/NBT 5% (magnification 10kX)

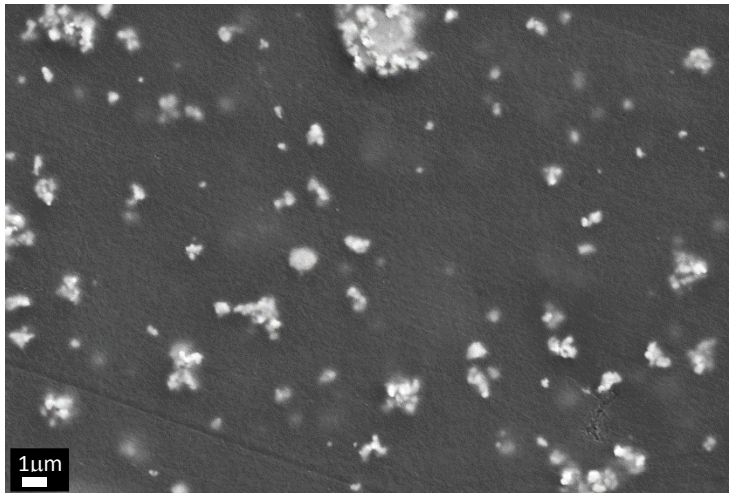


Fig.4.20: PVDF/NBT 10 % (magnification 10 kX)

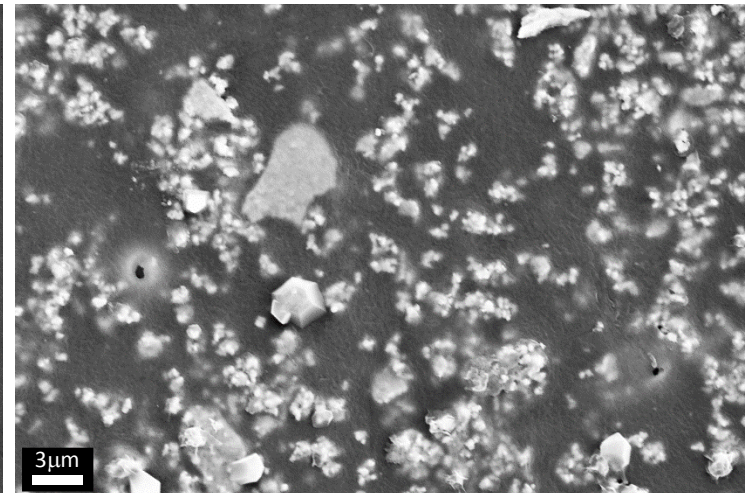


Fig.4.21: PVDF/NBT 20% (magnification 10 kX)

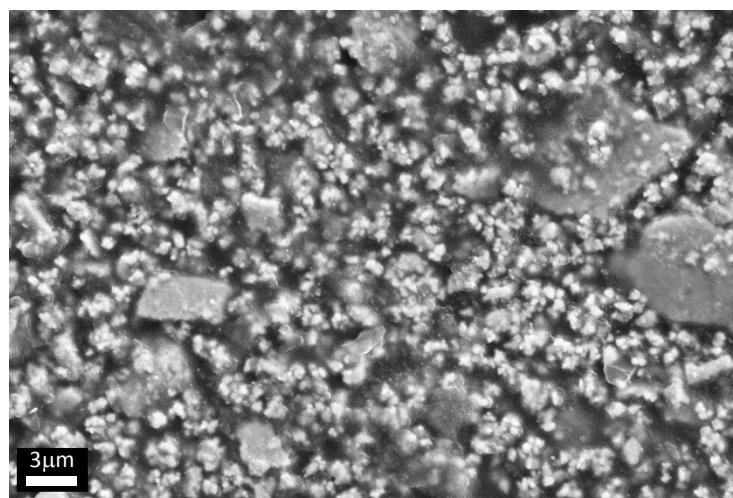


Fig.4.22: PVDF/NBT 30% (magnification 10kX)

SEM micrographs of PVDF are shown in Fig. 4.18, showing a smooth plain surface due to the presence of low atomic number elements. While from Fig. 4.19 to Fig. 4.22, the mass percentage of NBT in the composite is increased from 5%, 10%, 20%, and 30% respectively. The SEM micrographs show the dispersion of polycrystalline particles in the PVDF matrix. All the images are at 10KX magnification and the imaging was done by secondary electrons. The white color dots are NBT particles while the dark background is the PVDF matrix; it is observed that the dispersion of particles increases with the increase in mass fraction. The matrix gets denser with the mass percentage and at 30% NBT particles are totally dominating the composition as the matrix is rarely visible.

#### 4.2.3 Mechanical behavior of PVDF/NBT composite material

The matrix is of PVDF polymer and NBT ceramic powder particles are dispersed in it. The mass percentage of NBT particles is varied from 0 to 30%

1. PVDF film
2. Film PVDF/NBT 10%
3. Film PVDF/NBT 20%
4. Film PVDF/NBT 25%
5. Film PVDF/NBT 30%

The objective to study the material for mechanical properties by tensile testing was to calculate and observe the elastic behavior of composite material and later utilize it for vibration sensor applications.

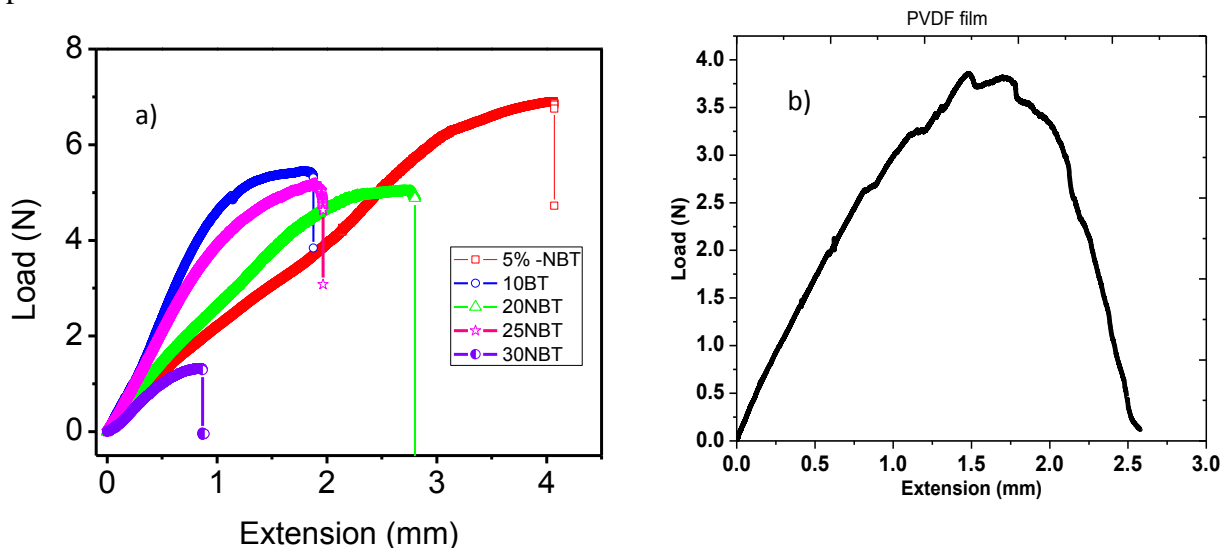


Fig.4.23 Preliminary results from tensile testing curve for PVDF/NBT composite films (a) and PVDF film (b).

From the figure 4.23 it is seen that as the NBT percentage increases the total extension of the specimen in mm, reduces. Simultaneously the load bearing capacity has increased for lower weight percentage and seen decreasing on increase of weight percentage further. The observed

features suggest possibilities on weaker interface between the particle and the polymer matrix. The typical behavior of semi crystalline polymer is shown in Fig.4.23 b) the humps in the curve as supposed to be due to crystallites in polymer. To conclude further on the mechanical property of the composite could be impossible without further sampling and detailed analysis.

# Chapter 5

## Studies on NBT as a Vibration Sensor

### 5.1 Introduction

Piezoelectric materials are used for vibration sensors, Acceleration sensor. The principle behind operation of charge based sensors is that change in applied pressure/ mass generates respective charge with relative amplitude. There are two types of piezoelectric sensor: high and low impedance. High-impedance based sensors have a charge output that requires a charge amplifier or external impedance converter for charge-to-voltage conversion. While Low-impedance types use the same piezoelectric sensing element as high-impedance units and also have built-in charge-to-voltage converter [39].

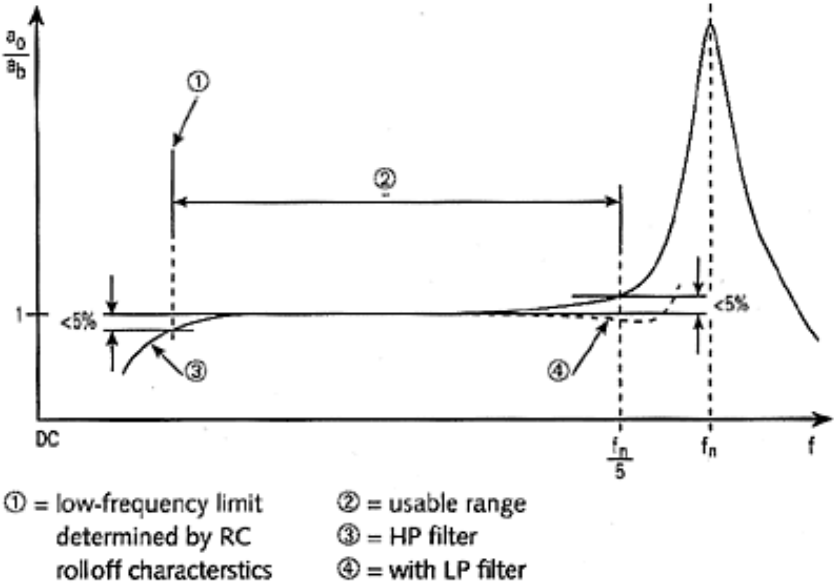


Fig.5.1 Typical frequency response curve for sensor [40]

The Fig. 5.1 explains the operating frequency range for any piezoelectric sensor. A sensor can be used for a maximum frequency up to the resonance value, above and below the usage range high pass (HP) filter and low pass (LP) filters are used for accurate calibration.



## 5.2 Experimental setup

The poled NBT pellet with silver paint electrodes was used to study the piezoelectric response. The objective was to detect the vibration generated by an active vibration source. So the sample was kept on a cantilever composite plate and a source was vibrating that plate with frequency of 10Hz as this source was connected to a frequency generator which is shown in Fig. 5.1. The NBT sample was connected to oscilloscope via BNC cable to collect the response. The principle of operation is just similar to accelerometer. A small mass was kept on top surface of pellet as at the time of vibration the mass presses the surface from top to generate charge and that generated signals were sent to oscilloscope (Tektronix TDS 2024C).

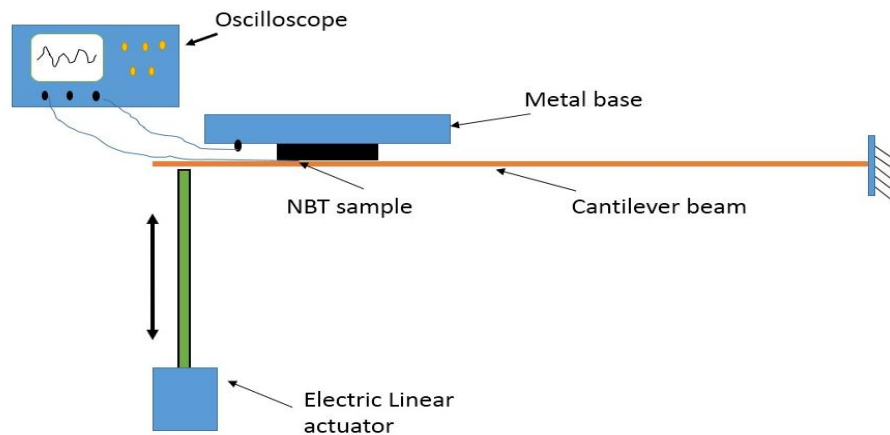


Fig. 5.2 Schematic diagram of the setup for vibration sensor

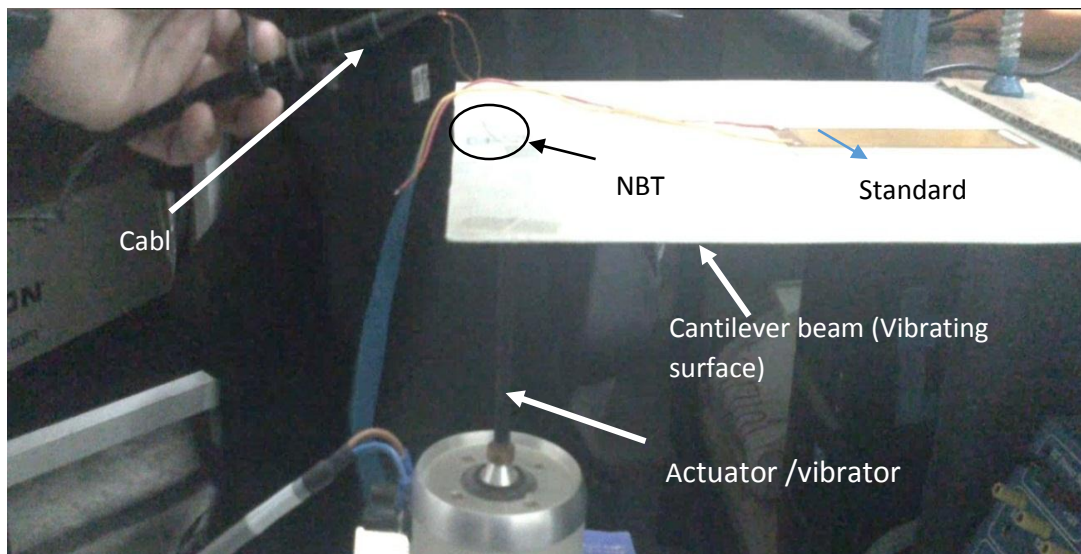


Fig. 5.2: Experimental setup for vibration sensing

In addition similar experiment was performed on commercially available piezoelectric (PZT) patch and the response was recorded for comparison.

### 5.3 Results of Vibration Sensor

The poled NBT sample with  $d_{33}$  74pC/N was used for making a setup for detecting the vibration of an active vibrating cantilever beam. Following in Fig is a graph it is clearly seen that there is a considerable response detected by the sample.

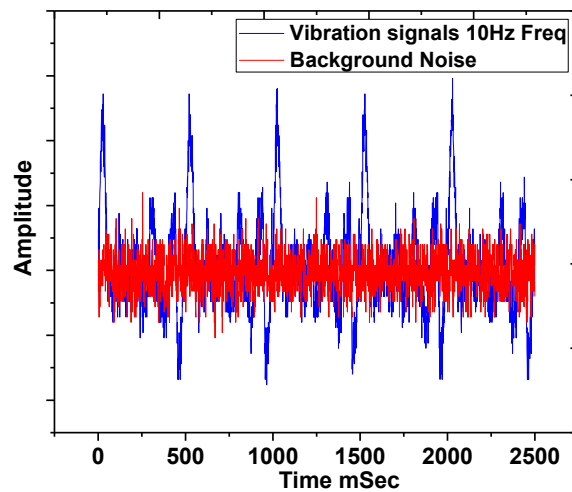


Fig. 5.3 Graph for comparison between received vibration signals and background noise.

The Fig. 5.3 shows the frequency response recorded by oscilloscope for a vibration of frequency 10Hz. The graph clearly shows the vibration response (blue lines) detected by NBT sensor and red region is response from background noise detected when there were no vibration.

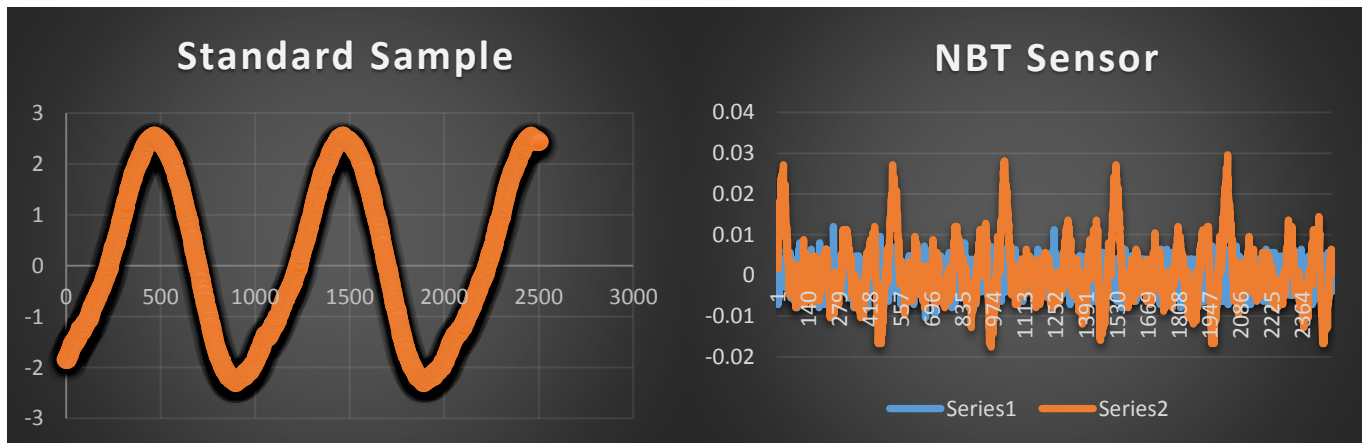


Fig. 5.4 Graphs of vibration response detected by an standard sample (left) and by NBT sensor (right)

From the comparison graphs it is observed that the difference in amplitude of response for NBT sensor is lesser by two order of magnitude, which could be due to the shape and processing effects involved on capturing the effects.

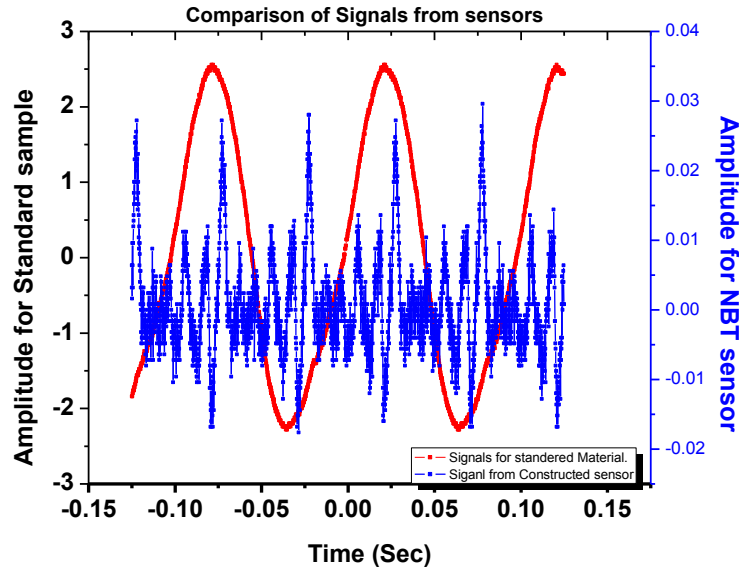


Fig. 5.5 comparison of vibration response between standard and constructed NBT sensor

### 5.3 Conclusion

The seismic vibrations have wide range of frequencies but the lower frequencies ranging from 0.1Hz to 1Hz causes larger damage to the structures. So it is very important to detect these lower frequencies. Though the response to vibration obtained from NBT sensor is lesser by two orders of magnitude, it provides potential response to be fabricated as a device. The signals can be amplified by adding external amplifier and signal conditioners to the circuit. Hence the NBT the lead free piezoelectric material can be used as a potential vibration sensor. Further standardization of the material is under progress.

# Chapter 6

## Summary and conclusion

### 6.1 Summary

In this thesis we have synthesized sodium bismuth titanate by solid state synthesis route and detailed studies on NBT for its structural and functional properties was done by X-ray diffraction, Raman spectroscopy, Dielectric measurements, and structural morphology by scanning electron microscopy. Similarly PVDF films and PVDF/NBT composite films were synthesized by solution casting technique and was characterized for its structural phase formation by X-Ray diffraction, SEM, and Raman spectroscopy. Finally the NBT samples were tested for detecting the vibration response.

### 6.2 Conclusions

#### A. NBT

- The formation of phase pure NBT polycrystalline powder has confirmed by XRD, SEM and Raman spectroscopy which similar to the earlier reported results.
- High relative density of 94% was achieved by controlling the parameters like calcination temperature, sintering temperature, compressing pressure for pellet making and the time of soaking while calcination and sintering.
- SEM micrographs show polycrystalline microstructure of NBT with an average grain size between 1 to 3 $\mu$ m.
- Dielectric measurement of NBT confirms Curie temperature at 320<sup>0</sup>C and the dielectric constant of ~2500 at 1 kHz frequency.
- Raman band for TiO<sub>6</sub> octahedra at 530cm<sup>-1</sup> and 580 cm<sup>-1</sup> confirms the perovskites structure of NBT.
- The d<sub>33</sub> value obtained for poled NBT sample at 74kV/cm electric field is 74pC/N. which is very much in comparison with the existing literature and also suitable for piezoelectric based device applications.
- The NBT pellet has shown positive piezoelectric response to detect vibration of 10Hz frequency. However, further optimization and standardization of the material is needed.

## **B. PVDF**

- The formation of  $\beta$ -PVDF phase at 90°C by annealing technique is confirmed by XRD.

## **C. NBT/PVDF composite**

- From tensile results for NBT/PVDF composite films it was clearly observed the decrease in elasticity with increase mass percentage of NBT particles.
- The XRD and Raman spectroscopy results for NBT/PVDF composite confirms that there is no new phase formation and there is coupling of the Raman bands at higher frequency of 800cm<sup>-1</sup>.

## **6.3 Future work**

As the work on NBT have given considerable results for lead free piezoelectric vibration sensor following work can be done on NBT and PVDF/NBT composites in future

1. Constructing a standard piezoelectric sensing device of NBT.
2. Calibrating the device for real life applications such as seismic wave measurement
3. Studying PVDF and PVDF/NBT films for piezoelectric response.

# References

1. Uchino, Kenji. "Advanced piezoelectric materials." *Science and Technology* 9 (2010).
2. Hong, Cheng-Shong, et al. "Effects of the MnO additives on the properties of  $\text{Pb}(\text{Fe}_{2/3}\text{W}_{1/3})\text{-PbTiO}_3$  relaxors: Comparison of empirical law and experimental results." *Journal of Applied Physics* 101.5 (2007): 054117-054117.
3. Jan Tichy. "Fundamental of piezoelectric sensorics" Springer-2010
4. <http://www.americanpiezo.com/>
5. Ye, Zuo-Guang, ed. *Handbook of advanced dielectric, piezoelectric and ferroelectric materials: Synthesis, properties and applications*. CRC Press, 2008.
6. J.S. Harrison, "Piezoelectric Polymers", NASA Langley Research Center, Hampton, Virginia, 2001
7. Takenaka, Tadashi, Hajime Nagata, and Yuji Hiruma. "Current developments and prospective of lead-free piezoelectric ceramics." *Japanese Journal of Applied Physics* 47 (2008): 3787.
8. Schwartz, Mel, ed. *Smart materials*. CRC Press, 2010.
9. Jones, G. O., and P. A. Thomas. "The tetragonal phase of  $\text{Na}_{0.5}\text{Bi}_{0.5}\text{TiO}_3$ -a new variant of the perovskite structure." *Acta Crystallographica Section B: Structural Science* 56, no. 3 (2000): 426-430.
10. Dorcet, V., and G. Trolliard. "A transmission electron microscopy study of the A-site disordered perovskite  $\text{Na}_{0.5}\text{Bi}_{0.5}\text{TiO}_3$ ." *Acta Materialia* 56, no. 8 (2008): 1753-1761.
11. Ramana, M. Venkata, S. Roopas Kiran, N. Ramamanohar Reddy, K. V. Siva Kumar, V. R. K. Murthy, and B. S. Murty. "Synthesis of lead free sodium bismuth titanate (NBT) ceramic by conventional and microwave sintering methods." *Journal of Advanced Dielectrics* 1, no. 01 (2011): 71-77.
12. Aksel, Elena, and Jacob L. Jones. "Advances in lead-free piezoelectric materials for sensors and actuators." *Sensors* 10, no. 3 (2010): 1935-1954.
13. Saïd, Senda, Pascal Marchet, Thérèse Merle-Méjean, and Jean-Pierre Mercurio. "Raman spectroscopy study of the  $\text{Na}_{0.5}\text{Bi}_{0.5}\text{TiO}_3\text{-PbTiO}_3$  system." *Materials letters* 58, no. 9 (2004): 1405-1409.
14. Barick, B. K., K. K. Mishra, A. K. Arora, R. N. P. Choudhary, and Dillip K. Pradhan. "Impedance and Raman spectroscopic studies of  $(\text{Na}_{0.5}\text{Bi}_{0.5})\text{TiO}_3$ ." *Journal of Physics D: Applied Physics* 44, no. 35 (2011): 355402.
15. Shashank Priya & Sahn Nahm, "Lead-Free Piezoelectrics", Springer (2012)

16. Fang, Zhigang Zak, ed. Sintering of advanced materials. Woodhead Publishing Limited, 2010.
17. Jin Soo Kim, Low-frequency Dielectric Dispersion and Impedance Spectroscopy of Lead-free  $\text{Na}_{0.5}\text{Bi}_{0.5}\text{TiO}_3$  (NBT) Ferroelectric Ceramics, Journal of the Korean Physical Society, Vol. 55, No. 2, August 2009
18. Senda et al, Relaxor behavior of low lead and lead free ferroelectric ceramic of the NBT-PT and NBT-KBT systems, Journal of European Ceramic Society 21(2001) 1333-1336
19. Gomah-Pettry, Jean-Richard, Senda Saïd, Pascal Marchet, and Jean-Pierre Mercurio. "Sodium-bismuth titanate based lead-free ferroelectric materials."Journal of the European Ceramic Society 24, no. 6 (2004): 1165-1169.
20. Suchanicz, Jan, Irena Jankowska-Sumara, and Tatiana V. Kruzina. "Raman and infrared spectroscopy of  $\text{Na}_{0.5}\text{Bi}_{0.5}\text{TiO}_3\text{-BaTiO}_3$  ceramics." Journal of electroceramics 27, no. 2 (2011): 45-50.
21. Sakata, Koichiro, and Yoichiro Masuda. "Ferroelectric and antiferroelectric properties of  $(\text{Na}_{0.5}\text{Bi}_{0.5})\text{TiO}_3\text{-SrTiO}_3$  solid solution ceramics."Ferroelectrics 7, no. 1 (1974): 347-349.
22. J.S. Harrison , "Piezoelectric Polymers", NASA Langley Research Center, Hampton, Virginia, 2001
23. Broadhurst, M. G., G. T. Davis, J. E. McKinney, and R. E. Collins. "Piezoelectricity and pyroelectricity in polyvinylidene fluoride—A model."Journal of applied physics 49, no. 10 (1978): 4992-4997.
24. Kawai, "The piezoelectricity of poly (vinylidene fluoride)", JAPAN.J. APPL. PHYS. 8 (1969) , 975-976
25. Nallasamy, P., and S. Mohan. "Vibrational spectroscopic characterization of form II poly (vinylidene fluoride)." Indian Journal of Pure and Applied Physics 43, no. 11 (2005): 821.
26. Gregorio Jr, R., and R. C. Capita. "Morphology and phase transition of high melt temperature crystallized poly (vinylidene fluoride)." Journal of materials science 35, no. 2 (2000): 299-306.
27. Daniel m. Esterly, "Manufacturing of poly(vinylidene fluoride) and evaluation of its mechanical properties", Virginia Polytechnic Institute and State University (2002)
28. Zhang, Yangyang, Shenglin Jiang, Maoyan Fan, Yike Zeng, Yan Yu, and Jungang He. "Piezoelectric formation mechanisms and phase transformation of poly (vinylidene fluoride)/graphite nanosheets nanocomposites." Journal of Materials Science: Materials in Electronics 24, no. 3 (2013): 927-932.
29. Furukawa, T., K. Ishida, and E. Fukada. "Piezoelectric properties in the composite systems of polymers and PZT ceramics." Journal of Applied Physics 50, no. 7 (1979): 4904-4912.
30. Dang, Z-M., L-Z. Fan, Y. Shen, and C-W. Nan. "Study on dielectric behavior of a three-phase  $\text{CF}/(\text{PVDF}+\text{BaTiO}_3)$  composite." Chemical physics letters 369, no. 1 (2003): 95-100.

31. Thomas, P., K. T. Varughese, K. Dwarakanath, and K. B. R. Varma. "Dielectric properties of Poly (vinylidene fluoride)/CaC<sub>3</sub>Ti<sub>4</sub>O<sub>12</sub> composites." *composites Science and Technology* 70, no. 3 (2010): 539-545.
32. Preparation and electroactive properties of a PVDF/nano-TiO<sub>2</sub> composite film, n. An et al. / *applied surface science* 257 (2011) 3831–3835
33. Ögüt, Erdem, O. Sinan Yördem, Yusuf Z. Menciloğlu, and Melih Papila. "Poly (vinylidene fluoride)/zinc oxide smart composite material." In *The 14th International Symposium on: Smart Structures and Materials & Nondestructive Evaluation and Health Monitoring*, pp. 65260Q-65260Q. International Society for Optics and Photonics, 2007.
34. Bowen, Leslie J., and Kenneth W. French. "Fabrication of piezoelectric ceramic/polymer composites by injection molding." In *Applications of Ferroelectrics, 1992. ISAF'92., Proceedings of the Eighth IEEE International Symposium on*, pp. 160-163. IEEE, 1992.
35. William D. Callister, Jr, "Materials Science and Engineering an Introduction", John Wiley & Sons, Inc.(2007)
36. S Satapathy et al, Effect of annealing on phase transition in poly (vinylidene fluoride) films prepared by using polar solvent, *bull. Mater. Sci.*, Vol.34, no 4, July 2011, pp. 727-733 Indian academy of sciences.
37. Pronin, I. P., P. P. Syrnikov, V. A. Isupov, V. M. Egorov, and N. V. Zaitseva. "Peculiarities of phase transitions in sodium-bismuth titanate." *Ferroelectrics* 25, no. 1 (1980): 395-397.
38. Levin, Igor, and Ian M. Reaney. "Nano-and Mesoscale Structure of Na<sub>1/2</sub>Bi<sub>1/2</sub>TiO<sub>3</sub>: A TEM Perspective." *Advanced Functional Materials* 22, no. 16 (2012): 3445-3452.
39. <http://www.sensorsmag.com/sensors/acceleration-vibration/the-principles-piezoelectric-accelerometers-1022>
40. <http://www.britannica.com/EBchecked/topic/176199/earthquake/59552/Properties-of-seismic-waves>